

Pion production

1 Introduction

We have seen that state-of-the-art self-consistent Hartree-Fock or shell model nuclear structure calculations are not able to correctly reproduce the binding energy of ^{11}Li or ^{14}Be . However, it is possible to numerically adjust the binding energy to the measured experimental values. In this case, one is able to reproduce the large observed interaction radii with reasonable accuracy [1]. The proton and neutron matter densities obtained in this way are represented by the solid lines in the lower part of Fig. 1(a).

Due to the small binding energy and the large spatial extension of the neutrons in the so-called “halo” [2], one expects the neutron momentum distribution to exhibit a smaller width than in more deeply bound nuclei. This has indeed been observed in several ways.

Kobayashi et al. [3] observed the fragmentation of ^{11}Li with a radioactive beam of energy 790 MeV/nucleon. Their experimental data for the transverse momentum distribution of ^9Li from the reaction $^{11}\text{Li} \rightarrow ^9\text{Li} + 2n$ can be found in the bottom half of Fig. 1(b). It can be fitted with a superposition of two Gaussian distributions of widths $\omega_{\text{core}} = 95 \pm 12$ MeV/c and $\omega_{\text{halo}} = 23 \pm 5$ MeV/c. By using Goldhaber’s statistical model of the fragmentation process [4], they were able to interpret the two widths as an indication that the neutron momentum distribution inside the halo and the core of ^{11}Li are different. However, alternative explanations of the two-widths shape of the transverse momentum distribution are possible [5]. It is therefore wise to pursue other complementary ways of determining the momentum and coordinate space structure of exotic nuclei. For example, one can also measure the neutron momentum distribution in ^{11}Li by detecting the neutrons from the decay of ^{11}Li [6, 7].

We will investigate the possibility to further determine the coordinate and momentum space distribution of neutrons inside weakly bound isotope via pion production with radioactive beams. In principle, pion production in nucleus-nucleus collisions can be described with nuclear transport models developed during the last decade [8, 9, 10]. These models have been very successful to describe particle production in heavy ion collisions. The most used model is based on the BUU equation. However, they are semi-classical in nature and therefore lack the capability to properly take into account the special nuclear structure features of weakly bound nuclei near the drip line. It is therefore necessary to construct a more phenomenological model. The model is not able to provide a complete time dependent description of heavy ion reactions the way the above mentioned transport models can. But it is more precise as far as utilizing nuclear structure information is concerned. Before, we have shown a calculation similar to the ones presented in Refs. [12, 13, 14], but using shell model nucleon densities and energy dependent cross sections. The calculations are due to Li, Bauer and Hussein [14].

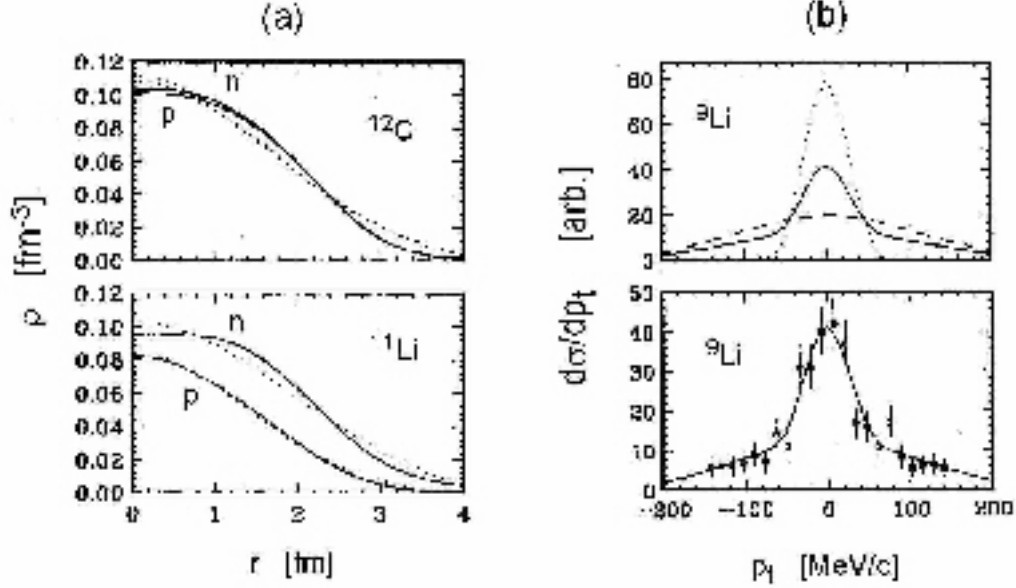


Figure 1 (a) Density distributions for ^{12}C and ^{11}Li . The solid lines are calculated with the binding energy adjusted shell model. The dotted lines are the Gaussian fits to the density profiles. (b) Upper figure: Calculated transverse momentum distribution of ^9Li in the reaction $^{11}\text{Li} + ^{12}\text{C} \rightarrow ^9\text{Li} + 2n + X$. The dashed (dotted) line is obtained by assuming knock out of two neutrons from the core (halo) of ^{11}Li . The solid line represents the weighted sum of the two. Lower figure: Comparison with the experimental data.

Supplement A

2 The Boltzmann equation for nucleon-nucleon collisions

Let us call $dN(\mathbf{r}, \mathbf{p}, t)$ the number of particles with positions \mathbf{r} and momenta \mathbf{p} at time t . If dN is the number of particles in the volume element d^3r and whose momenta fall in the momentum element d^3p at time t , then the *distribution function* $f(\mathbf{r}, \mathbf{p}, t)$ is given by

$$dN = f(\mathbf{r}, \mathbf{p}, t) d^3r d^3p \quad (1)$$

For a particle to be included in dN its position coordinates must lie between \mathbf{r}_i and $\mathbf{r}_i + \Delta\mathbf{r}_i$, and its momentum must lie between \mathbf{p}_i and $\mathbf{p}_i + \Delta\mathbf{p}_i$, where i runs from 1 to 3.

If there were no collisions, then a short time Δt later each particle would move from to $\mathbf{r} + \Delta\mathbf{r}$, and each particle momentum would change from to $\mathbf{p} + \mathbf{F}\Delta t$, where is \mathbf{F} the external force on a particle at \mathbf{r} with momentum \mathbf{p} . Therefore, any difference between $dN(\mathbf{r}, \mathbf{p}, t)$ and $dN(\mathbf{r} + \Delta\mathbf{r}, \mathbf{p} + \mathbf{F}\Delta t, t)$ is due to collisions, and we may set

$$[f(\mathbf{r} + \Delta\mathbf{r}, \mathbf{p} + \mathbf{F}\Delta t, t) - f(\mathbf{r}, \mathbf{p}, t)] d^3r d^3p = \left(\frac{\partial f}{\partial t} \right)_c d^3r' d^3p' \Delta t, \quad (2)$$

where $(\partial f/\partial t)_c$ is the time rate of change of f due to collisions. Expanding the first term on the left as a Taylor series about $f(\mathbf{r}, \mathbf{p}, t)$, we have (here repeated indices mean a summation, e.g., $a_i b_i = \mathbf{a} \cdot \mathbf{b} = a_1 b_1 + a_2 b_2 + a_3 b_3$)

$$f(\mathbf{r} + \Delta \mathbf{r}, \mathbf{p} + \mathbf{F} \Delta t, t) = f(\mathbf{r}, \mathbf{p}, t) + \left(\frac{\partial f}{\partial r_i} \frac{p_i}{m} + \frac{\partial f}{\partial p_i} F_i + \frac{\partial f}{\partial t} \right) \Delta t, \quad (3)$$

where m is the nucleon mass.

In the limit as $\Delta t \rightarrow 0$,

$$\frac{\partial f}{\partial r_i} \frac{p_i}{m} + \frac{\partial f}{\partial p_i} F_i + \frac{\partial f}{\partial t} = \left(\frac{\partial f}{\partial t} \right)_c \quad (4)$$

which is known as the *Boltzmann equation* for f . Note we have used the result that the Jacobian for the transformation $d^3 r' d^3 p' = |J| d^3 r d^3 p$ is unity, where J is the 6×6 element array,

$$J = \frac{\partial(x, y, z, p_x, p_y, p_z)}{\partial(x', y', z', p'_x, p'_y, p'_z)}. \quad (5)$$

This assumption is valid only if the collisions are elastic, i.e., if they conserve energy and momentum.

The system of nucleons are often free from external sources, so that one can drop off the term containing F_i in Eq. 4. However, to account for the effect of each particle interacting with all other, one introduces the concept of mean-field, $U(\mathbf{r}, \mathbf{p}, t)$. This mean-field exerts a force on each particle, given by $-\nabla_{\mathbf{r}} U(\mathbf{r}, \mathbf{p}, t)$. Re-deriving Eq. 4 in terms of a mean field yields

$$\frac{\partial f}{\partial t} + \left(\frac{\mathbf{p}}{m} + \nabla_{\mathbf{p}} U \right) \cdot \nabla_{\mathbf{r}} f - \nabla_{\mathbf{r}} U \cdot \nabla_{\mathbf{r}} f = \left(\frac{\partial f}{\partial t} \right)_c \quad (6)$$

Note that the left hand side of this equation is simply the total time derivative of the distribution function, Df/Dt . In the absence of collisions, one obtains the *Vlasov equation*

$$\frac{Df}{Dt} = \frac{\partial f}{\partial t} + \left(\frac{\mathbf{p}}{m} + \nabla_{\mathbf{p}} U \right) \cdot \nabla_{\mathbf{r}} f - \nabla_{\mathbf{r}} U \cdot \nabla_{\mathbf{r}} f = 0. \quad (7)$$

Let us now assume that the system of nucleons form a dilute system of particles. Dilute means that the total volume of the gas particles is small compared to the volume available to the gas,

$$na^2 \ll 1 \quad (8)$$

where n is the number density of particles and a is the radius of a particle. Since the particles in a neutral gas do not have long range forces like the particles in a plasma, they are assumed to interact only when they collide, i.e., when the separation between two particles is not much larger than $2a$. The term collision normally means the interaction between two such nearby particles. A particle moves in a straight line between collisions. The average distance traveled by a particle between two collisions is known as the mean free path. The mean free path depends on the cross section σ , and is given by

$$\lambda = \frac{1}{n\sigma}. \quad (9)$$

One consequence of the requirement that the gas be dilute is that $\lambda \gg a$. In other words the diluteness implies that the mean free path is much larger than the particle size so that a typical particle trajectory consists of long straight segments interrupted by almost discontinuous changes of direction when collisions occur. If the gas is dilute, the probability of three body collisions is much lower than for two body collisions and they can be neglected.

The Vlasov equation, $Df/Dt = 0$, says that f does not change as we move along the trajectory of a particle, provided collisions are neglected. Collisions can change f in two ways.

1. Some particles originally having momentum \mathbf{p} will have some different momentum after the collision. This causes a decrease in f .
2. Some particles having other momentum may have the momentum \mathbf{p} after a collision, increasing f .

The Boltzmann collisional term in the Boltzmann equation can be written as

$$\frac{Df}{Dt} d^3r d^3p = C_{in} - C_{out} \quad (10)$$

where C_{in} and C_{out} are the rates at which particles enter and leave the infinitesimal volume $d^3r d^3p$ due to collisions.

Suppose two particles with initial velocities \mathbf{v}_1 and \mathbf{v}_2 have velocities \mathbf{v}'_1 and \mathbf{v}'_2 and after a collision. Since all particles have the same mass, conservation of momentum and energy require that

$$\mathbf{v}'_1 + \mathbf{v}'_2 = \mathbf{v}_1 + \mathbf{v}_2 \quad \text{and} \quad \frac{1}{2} |\mathbf{v}'_1|^2 + \frac{1}{2} |\mathbf{v}'_2|^2 = \frac{1}{2} |\mathbf{v}_1|^2 + \frac{1}{2} |\mathbf{v}_2|^2 \quad (11)$$

One would like to calculate the final velocities \mathbf{v}'_1 and \mathbf{v}'_2 from the initial velocities. Since we have six components we need six equations to solve for them. Four are provided by the conservation equations. A fifth condition comes from the fact that collisions are coplanar if the forces between particles are purely radial, i.e., \mathbf{v}'_1 will lie in the plane of \mathbf{v}_1 and \mathbf{v}_2 , forcing \mathbf{v}'_2 to also lie in the same plane from conservation of momentum. We still need a sixth condition, which must come from the nature of the force between the particles. The short range nature of the forces allow us to assume that the collision occurs at essentially only one value of \mathbf{r} so we need not account for the changes of external forces. The unknown velocities are therefore specified once the impact parameter \mathbf{b} and the azimuthal orientation ϕ of the collision is known. For an elastic collision the magnitude of the relative velocity is a collisional invariant:

$$|\mathbf{v}'_1 - \mathbf{v}'_2| = |\mathbf{v}_1 - \mathbf{v}_2|, \quad (12)$$

which follows from kinetic energy conservation in the center of mass frame. Thus we may specify the remaining two pieces of information concerning the collision in terms of the change of the orientation of the relative velocity, i.e., in terms of two angles Θ and ϕ . In an elastic encounter the collision occurs in a single plane $\phi = \text{const.}$, turning the relative velocity $\mathbf{v}_1 - \mathbf{v}_2$ through an angle Θ without change in the magnitude of the relative velocity. For given intermolecular forces, the deflection, Θ , depends only on the impact parameter b . The

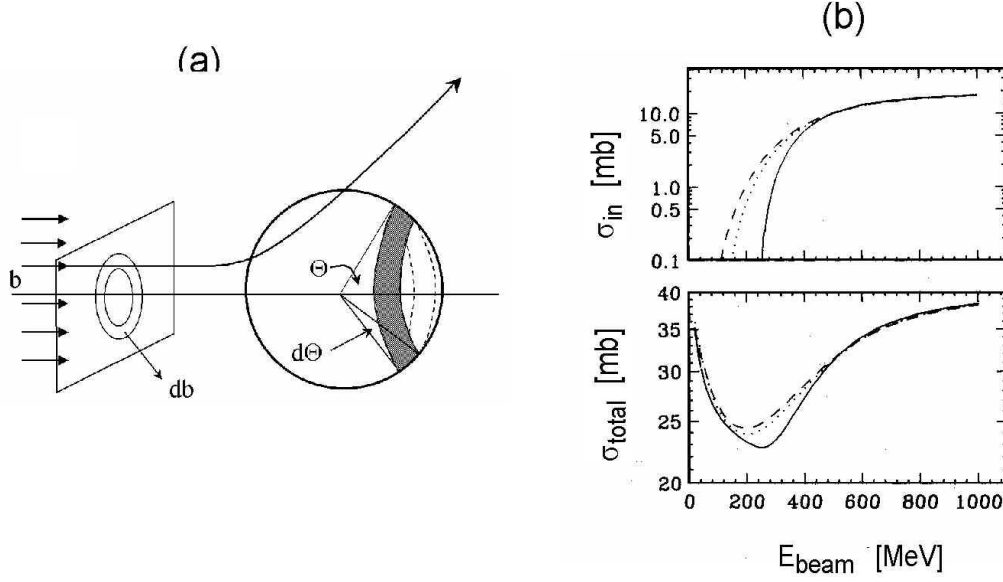


Figure 2 (a) Scattering of an incident beam of particles by a center of force. The impact parameter is b , and the angle of deflection is Θ . The number of particles scattered into a solid angle $d\Omega = 2\pi \sin \Theta d\Theta$ lying between Θ and $\Theta + d\Theta$ must equal the number scattered through impact parameters between b and $b + db$, hence $2\pi b db = 2\pi \sigma(\Theta) \sin \Theta d\Theta$. (b) Nucleon momentum averaged nucleon-nucleon cross sections in the reaction $^{11}\text{Li} + ^{12}\text{C}$. Solid lines are the free space nucleon-nucleon cross sections. Dotted lines are for carbon nucleons colliding with halo neutrons and dashed lines are for carbon nucleons colliding with core nucleons of ^{11}Li .

differential cross-section for the encounter $\sigma(\mathbf{v}_1, \mathbf{v}_2 | \mathbf{v}'_1, \mathbf{v}'_2)$ is defined so that $\sigma d\Omega = b db d\phi$, where $d\Omega = 2\pi \sin \Theta d\Theta$.

Consider a beam of particles of number density n_1 and velocity \mathbf{v}_1 colliding with another beam of particles of density n_2 and velocity \mathbf{v}_2 . A particle in the second beam experiences a flux $I = n_1 |\mathbf{v}_1 - \mathbf{v}_2|$ of particles from the first beam. We consider the number δn_c of collisions per unit time per unit volume which deflect particles from the second beam into a solid angle $d\Omega$,

$$\delta n_c = \sigma(\mathbf{v}_1, \mathbf{v}_2 | \mathbf{v}'_1, \mathbf{v}'_2) n_1 |\mathbf{v}_1 - \mathbf{v}_2| n_2 d\Omega. \quad (13)$$

Consider the inverse collision where $(\mathbf{v}_1, \mathbf{v}_2) \longrightarrow (\mathbf{v}'_1, \mathbf{v}'_2)$. If the molecular processes are time-reversible, then we expect the reverse cross-section to equal the forward cross-section:

$$\sigma(\mathbf{v}'_1, \mathbf{v}'_2 | \mathbf{v}_1, \mathbf{v}_2) = \sigma(\mathbf{v}_1, \mathbf{v}_2 | \mathbf{v}'_1, \mathbf{v}'_2) \quad (14)$$

It should be noted that this condition of time reversibility is by no means self-evident.

We now evaluate the term C_{out} . Consider the two streams of particles having the tips of their momentum vectors in d^3p_1 and d^3p_2 . The first stream makes up a beam of number density $n_1 = f(\mathbf{r}, \mathbf{p}_1, t) d^3p_1$, and velocity \mathbf{v}_1 , whereas the second stream constitutes a

beam of density $n_2 = f(\mathbf{r}, \mathbf{p}_2, t) d^3 p_2$ and velocity \mathbf{v}_2 . Substitution for n_1 and n_2 in the collision rate between the two beams is

$$\delta n_c = \sigma(\mathbf{v}_1, \mathbf{v}_2 | \mathbf{v}'_1, \mathbf{v}'_2) |\mathbf{v}_1 - \mathbf{v}_2| f(\mathbf{r}, \mathbf{p}_1, t) f(\mathbf{r}, \mathbf{p}_2, t) d\Omega d^3 p_1 d^3 p_2. \quad (15)$$

Since C_{out} must be equal to the number of collisions per unit time with the volume $d^3 r_1 d^3 p_1$, C_{out} is obtained by multiplying δn_c by $d^3 r_1$ and then integrating over all solid angles, Ω , and collision partner momenta, p_2 . Hence,

$$\begin{aligned} C_{out} &= d^3 r_1 \int_{p_2} \int_{\Omega} \delta n_c \\ &= d^3 r_1 d^3 p_1 \int d^3 p_2 \int d\Omega \sigma(\mathbf{v}_1, \mathbf{v}_2 | \mathbf{v}'_1, \mathbf{v}'_2) |\mathbf{v}_1 - \mathbf{v}_2| f(\mathbf{r}, \mathbf{p}_1, t) f(\mathbf{r}, \mathbf{p}_2, t). \end{aligned} \quad (16)$$

To evaluate C_{in} , we consider the reverse collisions between particles in $d^3 p'_1$ and with momenta in $d^3 p'_2$ such that their velocities after collisions lie within $d^3 p_1$ and $d^3 p_2$, respectively. The number of such collision per unit volume per unit time is

$$\delta n'_c = \sigma(\mathbf{v}'_1, \mathbf{v}'_2 | \mathbf{v}_1, \mathbf{v}_2) |\mathbf{v}'_1 - \mathbf{v}'_2| f(\mathbf{r}, \mathbf{p}'_1, t) f(\mathbf{r}, \mathbf{p}'_2, t) d\Omega d^3 p'_1 d^3 p'_2. \quad (17)$$

Recall that the relative velocity of the particles is a collisional invariant, $|\mathbf{v}'_1 - \mathbf{v}'_2| = |\mathbf{v}_1 - \mathbf{v}_2|$, and from *Liouville's theorem*, if the interaction can be described by a Hamiltonian,

$$d^3 p'_1 d^3 p'_2 = d^3 p_1 d^3 p_2 \quad (18)$$

Thus assuming reversible collisions, the invariance of the relative velocity and the constant phase space volume,

$$\delta n'_c = \sigma(\mathbf{v}_1, \mathbf{v}_2 | \mathbf{v}'_1, \mathbf{v}'_2) |\mathbf{v}_1 - \mathbf{v}_2| f(\mathbf{r}, \mathbf{p}'_1, t) f(\mathbf{r}, \mathbf{p}'_2, t) d\Omega d^3 p_1 d^3 p_2. \quad (19)$$

The term is C_{in} obtained by multiplying $\delta n'_c$ by $d^3 r_1$ and integrating over all solid angles, Ω , and collision partner momenta, \mathbf{p}_2 , i.e.,

$$C_{out} = d^3 r_1 d^3 p_1 \int d^3 p_2 \int d\Omega \sigma(\mathbf{v}_1, \mathbf{v}_2 | \mathbf{v}'_1, \mathbf{v}'_2) |\mathbf{v}_1 - \mathbf{v}_2| f(\mathbf{r}, \mathbf{p}'_1, t) f(\mathbf{r}, \mathbf{p}'_2, t). \quad (20)$$

Now that we have the rates at which particles leave and enter $d^3 r_1 d^3 p_1$ we can write the full *Boltzmann equation* as

$$\begin{aligned} \frac{\partial f}{\partial t} + \left(\frac{\mathbf{p}}{m} + \nabla_{\mathbf{p}} U \right) \cdot \nabla_{\mathbf{r}} f - \nabla_{\mathbf{r}} U \cdot \nabla_{\mathbf{r}} f = \\ \int d^3 p_2 \int d\Omega \sigma(\mathbf{v}_1, \mathbf{v}_2 | \mathbf{v}'_1, \mathbf{v}'_2) |\mathbf{v}_1 - \mathbf{v}_2| \\ \times [f(\mathbf{r}, \mathbf{p}'_1, t) f(\mathbf{r}, \mathbf{p}'_2, t) - f(\mathbf{r}, \mathbf{p}_1, t) f(\mathbf{r}, \mathbf{p}_2, t)]. \end{aligned} \quad (21)$$

which is conveniently abbreviated as

$$\frac{\partial f}{\partial t} + \left(\frac{\mathbf{p}}{m} + \nabla_{\mathbf{p}} U \right) \cdot \nabla_{\mathbf{r}} f - \nabla_{\mathbf{r}} U \cdot \nabla_{\mathbf{r}} f = \int d^3 p_2 \int d\Omega \sigma(\Omega) |\mathbf{v}_1 - \mathbf{v}_2| [f'_1 f'_2 - f_1 f_2]. \quad (22)$$

We have assumed that the differential cross-section is a function only of the scattering angle Ω between \mathbf{p}_1 and \mathbf{p}_2 , since the differential cross-section for a simple spherically symmetric interaction potential can, due to symmetry, only be a function of the scattering angle. The complete (classical) Boltzmann equation with the collision integral for binary collisions is a nonlinear integro-differential equation for the distribution function.

For a system of nucleons the classical Boltzmann equation can be modified to account for the Pauli principle. The principle states that no nucleon can scatter into a phase space already occupied by another nucleon. This amounts in modifying the term $f_1 f_2$ to $f_1 f_2 [1 - f'_1] [1 - f'_2]$, where the $1 - f'$ terms is zero if the final state is occupied ($f = 1$). Accordingly, $f'_1 f'_2$ is modified to $f'_1 f'_2 [1 - f_1] [1 - f_2]$. Thus, for a nucleon system of particles, the appropriate Boltzmann equation for a nucleon-nucleon collisions (called the *Boltzmann-Uehling-Uhlenbeck*, or *BUU*, equation) is

$$\begin{aligned} \frac{\partial f}{\partial t} + \left(\frac{\mathbf{p}}{m} + \nabla_{\mathbf{p}} U \right) \cdot \nabla_{\mathbf{r}} f - \nabla_{\mathbf{r}} U \cdot \nabla_{\mathbf{r}} f = \\ \int d^3 p_2 \int d\Omega \sigma_{NN}(\Omega) |\mathbf{v}_1 - \mathbf{v}_2| \\ \times \{ f'_1 f'_2 [1 - f_1] [1 - f_2] - f_1 f_2 [1 - f'_1] [1 - f'_2] \}. \end{aligned} \quad (23)$$

The collision integral, Eq.23, takes into account the nucleon scattering inside the nuclear medium. Its form can be justified on general physical grounds, but it can be also derived self-consistently from the quantum equations of motion of the one-body and two-body density .

Eq. 23 needs as basic ingredients the mean field U and the cross section σ_{NN} . Because these two quantities are related to each other, one should in principle derive them in a self-consistent microscopic approach, as the Brueckner theory. However, in practice the simulations are often done with a phenomenological mean field and free nuclear cross sections.

The most commonly used mean field is of Skyrme-type, eventually with a momentum dependent part [15].

The output of Eq. 23 is the distribution function $f(r, p, t)$, which allows one to calculate a lot of properties of the heavy-ion collisions. Let us quote collective flows, proton and neutron production rates, (sub-threshold and above threshold) pion and kaon yields, etc. Combining Eq. 23 with a phase-space coalescence model, one can also calculate such quantities as exclusive flows and intermediate fragment formations.

In order to numerically solve Eq. 23 one needs to go throughout the following general steps: initialization, mean field propagation, collisions and Pauli blocking. The solution of 23 is usually Monte Carlo simulated by using the pseudo-particle method. According to these models the dynamics is traced by the one-body distribution function $f(\mathbf{r}, \mathbf{p}, t)$ expanded in terms of a set of generating functions centered on a finite number of points, Monte Carlo distributed in the whole phase-space. In this way the dynamics of nucleons is replaced by the dynamics of test-particles. Between two collisions a test-particle propagates following a classical trajectory determined by Newton-type equations. In order to have a good approximation of the exact continuous distribution function, $f(\mathbf{r}, \mathbf{p}, t)$, the number of test-particles per nucleon should be large enough. This requirement brings about, in the case of a large nucleus, a fast increase of the CPU time needed for running serial-code simulations.

Let us briefly discuss the general aspects of a typical numerical algorithm. In the first step one prepares nuclei in the ground state by discretizing the continuous distribution function as a sum of elementary functions. Here we describe them in terms of Gaussian functions both in coordinate and momentum space, with fixed widths σ_r and σ_p :

$$f(\mathbf{r}, \mathbf{p}, t) = \frac{1}{n_g (4\pi^2 \sigma_r \sigma_p)^{3/2}} \sum_{i=1, n} \exp \left[-(\mathbf{r} - \mathbf{r}_i)^2 / 2\sigma_r^2 \right] \exp \left[-(\mathbf{p} - \mathbf{p}_i)^2 / 2\sigma_p^2 \right] \quad (24)$$

where n_g is the number of generating functions per nucleon. This number should be quite large in order to have a good approximation of the exact continuous distribution function $f(\mathbf{r}, \mathbf{p}, t)$. The total number of test-particles ("Gaussians") is $N = n_g A$, where A is the total number of nucleons in the nuclear system. The ground state is prepared by a Monte Carlo sampling of the phase space with a variational self-consistent procedure to reproduce the nuclear binding energy.

Once the initial phase-space configuration of the test particles in the two ground state nuclei is fixed, the two nuclei are translated and boosted to the center of mass frame where the calculation is performed. The evolution in time of the system is controlled by dividing the total reaction time in small time steps, dt (of the order of 0.5 fm/c). During a time step interval the test-particles are propagated freely in phase-space along the classical trajectories determined by the Newton equations, with the force term given by the derivative of the mean field. Actually, in the case of Gaussian generating functions (Eq. 24), it can be shown [16] that the dynamics of test-particles ("the Gaussians") is given by Ehrenfest type equations, with the force term replaced by the convoluted derivatives of the mean field over the given Gaussian:

$$\frac{d\mathbf{r}_i}{dt} = \frac{\mathbf{p}_i}{m} + \langle \nabla_p U(\mathbf{r}, \mathbf{p}) \rangle_{\mathbf{r}_i, \mathbf{p}_i} \quad \text{and} \quad \frac{d\mathbf{p}_i}{dt} = \frac{\mathbf{r}_i}{m} + \langle \nabla_r U(\mathbf{r}, \mathbf{p}) \rangle_{\mathbf{r}_i, \mathbf{p}_i} . \quad (25)$$

At the end of each time-step the phase space is searched for allowed collisions. The algorithm for simulating the collision integral is based on the mean free path, λ . The procedure is as follow [11]: for a given test particle one searches a possible scattering partner taken as the closest test-particle inside a sphere of a given radius. Then one estimates the averaged mean free path as $\lambda = (\rho\sigma)^{-1}$, where ρ is the local averaged density and is σ the cross section corresponding to the relative kinetic energy of the partners. Dividing the calculated mean free path by the relative velocity of the two test particles, one finds the averaged time-life between two collisions, dt_{coll} . In terms of dt_{coll} the probability for scattering is :

$$P = 1 - \exp(-dt/dt_{coll}) . \quad (26)$$

If dt is chosen as to have $dt \ll dt_{coll}$ then P can be approximated by dt/dt_{coll} . After the probability P is calculated the decision for the scattering is made by the Monte Carlo method: the scattering is decided if P is greater than a generated random number smaller than one. As soon as a collision is decided, the final momenta of the two scattered test-particles are randomly generated, with the momentum-energy conservation constraints. The final decision for the scattering is taken only if the final scattering states are not Pauli-blocked. The Pauli-blocking factor is $(1 - f_1)(1 - f_2)$ where f_1 and f_2 are the one-body distribution functions calculated in the phase-space points corresponding to the final states

of the scattered test-particles. The decision about the Pauli-blocking is taken again by Monte Carlo method.

3 Inclusive π^+ and π^- production cross section

Within a Glauber-type multiple collision model, the total number of nucleon-nucleon collisions in the reaction of $A + B$ at an impact parameter b is

$$N(b) = \bar{\sigma}(E) \int_{\mathcal{O}} dx dy \int dz_1 dz_2 \rho_A(x, y, z_1) \rho_B(x, y - b, z_2), \quad (27)$$

where \mathcal{O} is the overlap region of nuclei A and B , and $\bar{\sigma}(E)$ is the momentum averaged total nucleon-nucleon cross section. Since the core nucleons and the halo neutrons have different momentum distributions in ^{11}Li , $\bar{\sigma}(E)$ may be written as

$$\bar{\sigma}(E) = \frac{9}{11} \bar{\sigma}_{\text{core}}(E) + \frac{2}{11} \bar{\sigma}_{\text{halo}}(E). \quad (28)$$

Since we wish to analytically carry out the bulk of the calculations, we follow Karol [17] and assume that the nucleon density distribution is a Gaussian function

$$\rho(r) = \rho(0) \exp\left(-\frac{r^2}{a^2}\right). \quad (29)$$

The integration in Eq. 27 can then be performed analytically to yield the result

$$N(b) = \frac{\bar{\sigma}(E) \pi^2 \rho_A(0) \rho_B(0) a_A^3 a_B^3}{a_A^2 + a_B^2} \exp\left(-\frac{b^2}{a_A^2 + a_B^2}\right). \quad (30)$$

Similar forms for the proton-proton and neutron-neutron collision numbers can be obtained in terms of their density distribution parameters.

Under the assumption that pions are produced through Δ resonances, the inclusive π^+ and π^- cross sections can then be written as [13]

$$\begin{aligned} \frac{d\sigma_{\text{inc}}^{\pi^+}}{d\Omega} &= |f_{N\Delta}(q)|^2 Z_A Z_B \frac{\pi^2 \rho_{ZA}(0) \rho_{ZB}(0) a_{ZA}^3 a_{ZB}^3}{a_{ZA}^2 + a_{ZB}^2} \\ &\times 2\pi \int_0^\infty b db \exp\left[-\frac{b^2}{a_{ZA}^2 + a_{ZB}^2} - \frac{\bar{\sigma}(E)(AB-1)\rho_A(0)\rho_B(0)a_A^3 a_B^3}{a_A^2 + a_B^2} \right. \\ &\quad \left. \exp\left(-\frac{b^2}{a_A^2 + a_B^2}\right) \right], \end{aligned} \quad (31)$$

$$\begin{aligned} \frac{d\sigma_{\text{inc}}^{\pi^-}}{d\Omega} &= |f_{N\Delta}(q)|^2 N_A N_B \frac{\pi^2 \rho_{NA}(0) \rho_{NB}(0) a_{NA}^3 a_{NB}^3}{a_{NA}^2 + a_{NB}^2} \\ &\times 2\pi \int_0^\infty b db \exp\left[-\frac{b^2}{a_{NA}^2 + a_{NB}^2} - \frac{\bar{\sigma}(E)(AB-1)\rho_A(0)\rho_B(0)a_A^3 a_B^3}{a_A^2 + a_B^2} \right. \\ &\quad \left. \exp\left(-\frac{b^2}{a_A^2 + a_B^2}\right) \right], \end{aligned} \quad (32)$$

where ρ_{Ni} and ρ_{Zi} are the neutron and proton coordinate space densities of nucleus i , and $f_{N\Delta}(q)$ is the amplitude for the process $N+N \rightarrow N+\Delta$. The exponentials inside the integrals represent the product of the proton (Eq. 31) or neutron (Eq. 32) densities with the elastic survival probability given by $\exp[-(\bar{\sigma}(E)(AB-1)\rho_A(0)\rho_B(0)a_A^3a_B^3)/(a_A^2+a_B^2)] \exp(-$

At beam energies smaller than 1 GeV/nucleon, available experimental data [18, 19] show that pions are mainly produced through Δ resonances. Direct processes of the form $N+N \rightarrow N+N+\pi$ account for less than 20 percent and higher resonances have negligible cross sections.

From the experimental data of n+p collisions [18] and the calculated ratio of the isospin matrix elements [13], it can be shown that the numbers of π^+ and π^- produced in n+p collisions are smaller than that in p+p and n+n collisions, respectively, by about an order of magnitude. We therefore expect that the above equations are good approximations for the present purpose of this calculation.

The above considerations do not include the effect of the Pauli-exclusion principle on the final state nucleons after producing the pions. This should result in a reduction of $|f_{N\Delta}(q)|^2$ in the nuclear medium. However, to first approximation, this reduction should be the same for both pion species, and since we are only interested in the ratio of the production cross sections, the reduction factor will cancel out.

Pion reabsorption accounts for up to 50% of the produced primordial pions in the light systems studied here [9]. In the same spirit as just described for the Pauli exclusion principle, the amplitudes $f_{N\Delta}$ should be understood as effective amplitudes which already include this reduction.

Since we are interested in the ratio of the inclusive π^+ and π^- production, the main ingredients in the model calculation are then the density parameters and the momentum averaged cross sections.

We start out by looking for realistic density distributions for protons and neutrons for all isotopes under consideration. This is accomplished by using a binding energy adjusted shell model program [1]. As examples for the calculated density distributions, we display in Fig. 1(a) the neutron and proton densities for ^{12}C (upper part) and ^{11}Li (lower part) by the solid lines.

The results of the Gaussian fit to the calculated density distributions are represented by the dotted lines. In Table 9.1, we list the obtained values for $\rho(0)$ and a for proton and neutron density distributions for all Li-isotopes used in the subsequent calculations as well as the corresponding values for ^{12}C .

	$\rho_n(0)$ (fm $^{-3}$)	a_n (fm)	$\rho_p(0)$ (fm $^{-3}$)	a_p (fm)	$\rho(0)$ (fm $^{-3}$)	a (fm)
^{12}C	0.1148	2.110	0.1120	2.128	0.2268	2.120
^7Li	0.1051	1.897	0.1121	1.688	0.2168	1.797
^8Li	0.1151	1.984	0.0996	1.755	0.2134	1.885
^9Li	0.1215	2.071	0.0989	1.760	0.2178	1.952
^{11}Li	0.1115	2.346	0.0851	1.851	0.1922	2.175

Table 9.1: Parameters of the Gaussian fits to the nucleon density distributions in Li-isotopes and ^{12}C .

For calculating the momentum averaged nucleon-nucleon cross sections, one chooses the momentum space distribution functions such that the results agree with know experimental data.

One such comparison is performed in Fig. 1(b). In the upper part, one uses a Fermi gas model for the momentum distribution of the neutrons in ^{11}Li . One assumes different Fermi momenta for core and halo neutrons. The fitted values are $P_F(\text{core}) = 158 \text{ MeV}/c$ and $P_F(\text{halo}) = 38 \text{ MeV}/c$ which coincide with the one inferred from the experimental data by using the Goldhaber model. By randomly picking 2 neutron momenta from within these Fermi spheres and adding their momenta, one obtains a recoil spectrum for ^9Li in the projectile rest frame, employing the assumptions entering the Goldhaber model [4]. By picking two neutrons from the halo, one obtains the dotted curve in Fig. 1(b). The dashed curve is the result of using the same procedure on two core neutrons. The solid curve is the result of an addition of the two contributions with the proper weights as measured in the experiment of Kobayashi et al. [3]. For purposes of comparison, all curves in the upper part of Fig. 1(b) were normalized to the same value. In the lower part of this figure, we compare the simulated ^9Li transverse momentum spectra to the data of Kobayashi et al. [3]. One can see that one is able to reliably fit the experimental observables.

We obtain the momentum distribution averaged nucleon-nucleon cross sections by integrating $\sigma(\sqrt{s})$ weighted with the momentum distributions of target and projectile,

$$\bar{\sigma}(E_{\text{beam}}) = \int f_A(\mathbf{p}_A) f_B(\mathbf{p}_B - \mathbf{p}_{\text{beam}}) \sigma(\sqrt{s}(\mathbf{p}_A, \mathbf{p}_B)) d^3 p_A d^3 p_B. \quad (33)$$

Here, $f_i(\mathbf{p})$ are the momentum distributions of target ($i = A$) and projectile $i = B$.

For the purpose of this calculation, one can use the well known parametrizations of Cugnon [20] for the free space elastic and inelastic nucleon-nucleon cross sections as a function of the available center of mass energy, \sqrt{s} , in a nucleon-nucleon collision.

$$\begin{aligned} \sigma_{\text{el}}(\sqrt{s}) &= \frac{35}{1 + 100(s - 1.8993)} + 20, \quad (\sqrt{s} > 1.8993) \\ \sigma_{\text{inel}}(\sqrt{s}) &= \frac{20(\sqrt{s} - 2.015)^2}{0.015 + (\sqrt{s} - 2.015)^2}, \quad (\sqrt{s} > 2.015). \end{aligned} \quad (34)$$

In this parameterization, \sqrt{s} is measured in GeV and σ in mb.

In Fig. 2(b), we display the results for $\bar{\sigma}_{\text{inel}}(E_{\text{beam}})$ and $\bar{\sigma}_{\text{total}}(E_{\text{beam}})$ for three different cases. The solid lines are for free nucleons. In this case, the distribution function f are δ -functions, and we have $\bar{\sigma}(E_{\text{beam}}) = \sigma_{NN}$. The threshold energy for pion production is in this case $E_{\text{beam}}^{\text{th}}/\text{nucleon} = 290 \text{ MeV}$.

The dashed and dotted lines represent the case that the target is a carbon nucleus. $f_A(\mathbf{p})$ is then a Fermi gas distribution function with Fermi momentum of 221 MeV/c determined from the carbon fragmentation experiment. The dashed lines are obtained by using the momentum distribution of ^{11}Li core neutrons for f_B , and the dotted line represents the case that the halo neutron momentum distribution is

used. In these cases, the threshold energies for pion production are 70 MeV and 120 MeV, respectively.

One can see from Fig. 2(b) that the distribution averaged value of the total nucleon-nucleon cross section is hardly affected by the momentum distribution of nucleons in target and projectile. However, the averaged inelastic cross section shows a very large effect close to the threshold.

In Table 9.2, one sees the results for the ratio

$$E = \frac{\sigma_{\text{inc}}^{\pi^-} - \sigma_{\text{inc}}^{\pi^+}}{\sigma_{\text{inc}}^{\pi^-} + \sigma_{\text{inc}}^{\pi^+}} \quad (35)$$

for the systems ${}^A\text{Li} + {}^{12}\text{C}$ ($A = 7, 8, 9, 11$) with $\bar{\sigma} = 40$ mb and 25 mb. These two values for $\bar{\sigma}$ are chosen to represent the case for nucleus-nucleus interactions around the pion production threshold ($E_{\text{beam}} \approx 200$ MeV/nucleon $\rightarrow \bar{\sigma} \approx 25$ mb) and for reactions at higher beam energies ($E_{\text{beam}} \approx 800$ MeV/nucleon $\rightarrow \bar{\sigma} \approx 40$ mb). For comparison, we also present the ratio E_0 for the two cross section which results from simple counting arguments of neutrons and protons or, equivalently, from assuming that protons and neutrons have the same density distribution in Eq. 35,

$$E_0 = \frac{N_A N_B - Z_A Z_B}{N_A N_B + Z_A Z_B}. \quad (36)$$

The ratio E is sensitive to the difference between proton and neutron density distribution [12].

	${}^7\text{Li}+{}^{12}\text{C}$	${}^8\text{Li}+{}^{12}\text{C}$	${}^9\text{Li}+{}^{12}\text{C}$	${}^{11}\text{Li}+{}^{12}\text{C}$
$E(40\text{mb})$	0.1153	0.2221	0.2955	0.3951
$E(25\text{mb})$	0.1143	0.2210	0.2939	0.3927
E_0	0.1429	0.2500	0.3333	0.4545

Table 9.2: Comparison of the computed normalized cross section differences between negative and positive pion production, E , for two different values of $\bar{\sigma}$ and the same quantity obtained from simple counting of nucleons, E_0 , for reactions of different Li isotopes with ${}^{12}\text{C}$.

4 Pion energy spectra

If we want to study pion energy spectra, it is clearly not sufficient any more to use energy averaged production cross sections. In an exploratory study of pion spectra with exotic nuclei, a modified Fermi gas model can be used. It was first used by G. Bertsch in the study of threshold pion production [21].

For the individual nuclei, we assume that the phase space distribution function can be separated into coordinate and momentum parts. For the momentum space distribution of the colliding nuclei we use a simplified form of two homogeneously filled Fermi spheres, the centers of which are separated by the beam momentum

$$f_{AB}(\mathbf{p}) = \theta(p_{f_A} - |\mathbf{p}|)A + \theta(p_{f_B} - |\mathbf{p} - \mathbf{p}_{\text{beam}}|)B. \quad (37)$$

Here p_{f_A} and p_{f_B} are the Fermi momenta of the projectile of mass A and target of mass B respectively. We will use the Fermi momenta for carbon and ^{11}Li extracted from the experimental data as we have discussed in the previous Section.

Pion energy spectra in the reaction $A + B$ can then be calculated as a sum of the pion energy distribution in each nucleon-nucleon collision with all possible momenta within the Fermi spheres

$$\left(\frac{d\sigma_\pi}{dE}\right)_{AB} = C \int \left(\frac{d\sigma_\pi(s)}{dE}\right)_{NN} f_A(\mathbf{p}_A) f_B(\mathbf{p}_B) d^3p_A d^3p_B, \quad (38)$$

where C is a constant coming from the integration over the impact parameter, which is irrelevant for the following discussions. s is the square of the center of mass energy of the two colliding nucleons.

To calculate the pion energy distribution $(d\sigma_\pi/dE)_{NN}$ in each nucleon-nucleon collision, we assume that pion production is proceeding via the Δ resonance. The mass distribution of the Δ resonance is taken from Y. Kitazoe et. al. [19] and is given by

$$P(M_\Delta) = \frac{0.25 \Gamma^2(q)}{(M_\Delta - M_0)^2 + 0.25 \Gamma^2(q)}, \quad (39)$$

where $M_0 = 1232$ MeV, and the width $\Gamma(q)$ of the resonance is parametrized as

$$\Gamma(q) = \frac{0.47q^3}{[1 + 0.6(q/m_\pi)^2] m_\pi^2}. \quad (40)$$

q is the pion-momentum.

The Δ is assumed to be produced isotropically in the nucleon-nucleon center of mass frame, and one can also assume that the decay of the resonance has an isotropic angular distribution in the Δ rest frame. The decay of the resonance can then be calculated using a Monte Carlo integration technique. This leads to a pion energy spectrum in the Δ rest frame which is finally Lorentz transformed into the laboratory frame.

The integration in Eq. 38 for calculating the pion spectra in the reaction $A + B$ can be performed with a Monte Carlo integration method. One generates pairs of colliding nucleons from the projectile and the target, and isospin quantum numbers are assigned to these nucleons according to the N/Z ratios of the projectile and the target. Then, one can use available experimental data [18, 22] for pion production cross sections in nucleon-nucleon collisions in all possible isospin channels.

One such calculation is performed for the reaction $^{11}\text{Li} + ^{12}\text{C}$ at various beam energies. To show the sensitivity of the pion energy spectra on the nucleon momentum distribution of the radioactive nuclei, Fig. 3(a) shows the π^- spectra calculated by using the core Fermi momentum and halo Fermi momentum for the ^{11}Li projectile, respectively. The solid histograms are calculated with $p_{f_A} = p_f(\text{halo}) = 38$ MeV/c and the dotted histograms are calculated with $p_{f_A} = p_f(\text{core}) = 158$ MeV/c. These two calculations simulate the situations that nucleons coming from ^{12}C collide with the halo and core nucleons of the ^{11}Li , respectively [14].

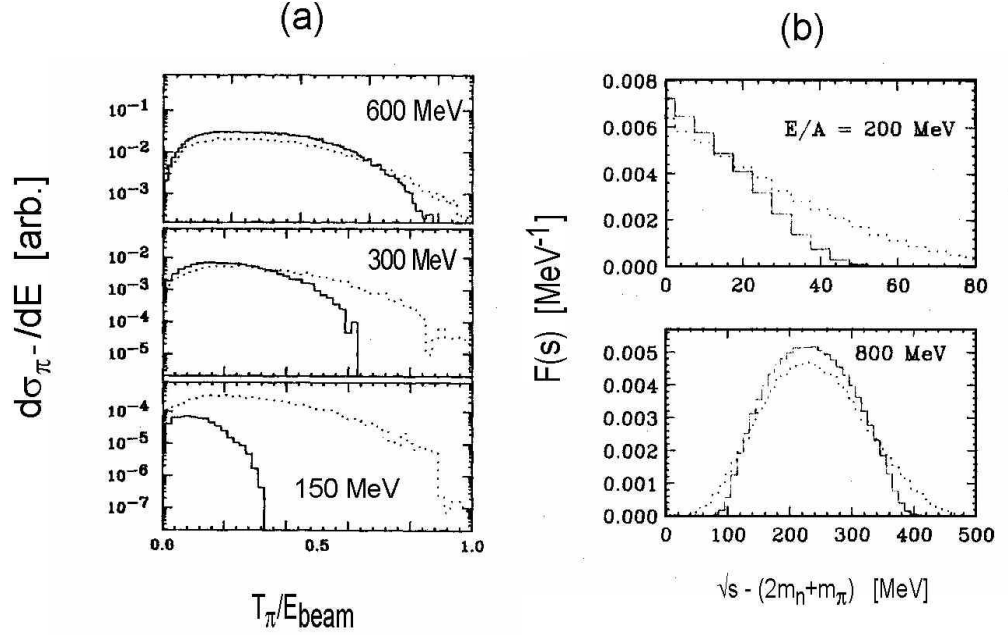


Figure 3 (a) π^- kinetic energy spectra in the reaction $^{11}\text{Li}+^{12}\text{C}$ at beam energies of 600, 300 and 150 MeV/nucleon. The solid lines are calculated with $p_{fA} = p_f(\text{halo})$ and the dotted lines are calculated with $p_{fA} = p_f(\text{core})$. (b) Distribution of the center of mass energy above pion production threshold for pairs of colliding nucleons in the reaction $^{11}\text{Li}+^{12}\text{C}$. The solid and dotted lines are calculated under the same conditions as in (a).

A strong sensitivity of the pion spectra to the nucleon momentum distribution can be seen, in particular for beam energies smaller than about 300 MeV/nucleon. Moreover, the different slopes of the two curves indicate that the different momentum distributions of core and halo neutrons can be seen experimentally.

Of course, one needs to know how to disentangle the pions produced by the core and by the halo neutrons. One can do this in two ways: First, one can separate central and peripheral collisions via some impact parameter trigger. Since the halo neutrons should contribute stronger to pion production in peripheral collisions, their effect can be isolated. A second and more tractable way to isolate the effect of the halo neutrons is a subtraction method. Here one can utilize the fact that a ^9Li nucleus contains the same core neutrons as ^{11}Li . Thus, if one subtracts the pion spectrum produced in a ^9Li induced reaction from that of a ^{11}Li induced and otherwise identical reaction, the pion spectrum due to the halo neutrons can be obtained.

Presently available radioactive beam facilities can produce high quality ^{11}Li and ^9Li beams. Using these, the different neutron momentum distributions of core and halo neutrons in ^{11}Li shows up as contributions to the pion energy spectra with different slopes in ^{11}Li and ^9Li induced reactions. One estimates [14] that a beam of 10^5 ^{11}Li per second at a beam energy of 300 MeV/nucleon would produce about 10^4

pions per second. With this production rate, a high quality experiment using a pion spectrometer can be performed.

As can be seen from Fig. 3(a), the difference in the slope of the pion spectra is not so obvious at beam energies above 600 MeV/nucleon. This can be understood by looking at the distribution of the center of mass energy, \sqrt{s} , of the two colliding nucleons in the reaction $A + B$

$$F(s) = \int f_A(\mathbf{p}_A) f_B(\mathbf{p}_B - \mathbf{p}_{beam}) \delta(s - 2m_n^2 - 2E_A E_B + 2\mathbf{p}_A \cdot \mathbf{p}_B) d^3 p_A d^3 p_B. \quad (41)$$

Here we take on-shell nucleons so that $E_i = (p_i^2 + m_n^2)^{1/2}$ for $i = A, B$.

In Fig. 3(b) we present the distribution of $\sqrt{s} - (2m_n + m_\pi)$, which is the total available center of mass energy above pion production threshold in nucleon-nucleon collisions. The calculation was done [14] for the reaction $^{11}\text{Li} + ^{12}\text{C}$ at beam energies of 200 MeV/nucleon and 800 MeV/nucleon. Again, the solid histograms are the results using $p_{f_A} = p_f(\text{halo})$ and the dotted ones using $p_{f_A} = p_f(\text{core})$. The effect of different internal momentum distributions is obvious at lower energies, but as the beam energy gets much larger than the pion production threshold energy, the effect becomes less obvious.

One can thus see that pion production with radioactive nuclei provides an alternative way for further determination of the properties of exotic nuclei.

5 References

1. G.F. Bertsch, B.A. Brown and H. Sagawa, Phys. Rev. C **39** (1989) 1154.
2. P.G. Hansen and B. Jonson, Europhys. Lett. **4** (1987) 409.
3. T. Kobayashi et al., Phys. Rev. Lett. **60** (1988) 2599.
4. A.S. Goldhaber, Phys. Lett. **53B** (1974) 306.
5. C.A. Bertulani and M.S. Hussein, Phys. Rev. Lett. **64** (1990) 1099.
6. R. Anne, S.E. Arnell, R. Bimbot, H. Emling, D. Guillemaud-Mueller, P.G. Hansen, L. Johannsen, B. Jonson, M. Lewitowicz, S. Mattsson, A.C. Mueller, R. Neugart, G. Nyman, F. Pougheon, A. Richter, K. Riisager, M.G. Saint-Laurent, G. Schrieder, O. Sorlin and K. Wilhelmsen, Phys. Lett. **B250** (1990) 19.
7. D. Guillemaud-Müller and A.C. Müller, "NSCL Seminars on Experimental Techniques: 1. Exotic Nuclei", Michigan State University Report MSUCL-742.
8. B.-A. Li and W. Bauer, Phys. Lett. **B254** (1991) 335.
9. W. Bauer, Phys. Rev. **C40** (1989) 715.
10. W. Cassing, et al., Phys. Rep. **188** (1990) 363.
11. A. Bonasera, F. Gulminelli and J. Molitoris, Phys. Rep. **243** (1994) 1.
12. R.J. Lombard and J.P. Maillet, Europhys. Lett. **6** (1988) 323.
13. A. Tellez, R.J. Lombard and J.P. Maillet, J. Phys. **G13** (1987) 311.
14. B.-A. Li, W. Bauer and M.S. Hussein, Nucl. Phys. **A533** (1991) 749.
15. C.Gale, G.Bertsch and S. Das Gupta, Phys. Rev. **C35** (1987)1666.

16. C. Gregoire et al, Nucl.Phys. **A465** (1987)317.
17. P.J. Karol, Phys. Rev. **C11** (1975) 1203.
18. B.J. VerWest and R.A. Arndt, Phys. Rev. **C25** (1980) 1979.
19. Y. Kitazoe et. al., Phys. Lett. **166B** (1986) 35.
20. J. Cugnon, T. Mizutani and J. Vandermeulen, Nucl. Phys. **A352** (1981) 505.
21. G.F. Bertsch, Phys. Rev. **C15** (1977) 713.
22. W.O. Lock and D.F. Measday, Intermediate Energy Nuclear Physics (Methuen, London, 1970).

6 Introduction

The parity nonconserving (PNC) nucleon interaction in nuclei caused by the PNC Weak interaction, and PNC effects in neutron-nucleus reactions are subject of interest for both experimentalists and theorists [1, 2, 3, 4, 5, 6, 7, 8, 9]. The overall scale of the observable PNC effects is found to be in reasonable agreement with estimates in existing theory of the weak interactions [1] based on the Standard Model. Complete understanding of PNC forces in nuclear domain, which requires reliable QCD-based models of hadrons is far from being reached. This motivates extensive studies of the strengths of the PNC forces.

The PNC effects have been probed in normal nuclei. Physics of exotic nuclei studied with unstable nuclear beams [10, 11, 12, 13, 14, 15, 16, 17, 18, 20, 21, 22, 23] appears to be one of the most promising modern nuclear areas. Due to their specific structure, exotic nuclei, e.g., halo nuclei can offer new possibilities to probe those aspects of nuclear interactions which are not accessible with normal nuclei. It is therefore interesting to examine possibilities of using exotic nuclei to investigate the effects of violation of fundamental symmetries, i.e., spatial parity and time reversal.

Some aspects of the Weak interactions in exotic nuclei have been discussed in literature [17, 18] in relation to the beta decay and to possibilities to study the parameters of the Cabibbo-Kobayashi-Maschawa matrix.

The aim of the next sections is to present a simple evaluation of the magnitude of the PNC effects in halo nuclei, following Hussein et al. [19]. We confine ourselves to the case of nucleus ^{11}Be , the most well studied, both experimentally and theoretically [10, 11, 12, 15, 16]. One finds that the ground state, the $2s_{1/2}$ halo configuration, acquires admixture of the closest in energy halo state of opposite parity, $1p_{1/2}$. This effect originates from the weak interaction of the external halo neutron with the core nucleons in the nuclear interior. As a result, the neutron halo cloud surrounding the nucleus acquires the wrong parity admixtures that may be tested in experiments which can probe the halo wave functions in the exterior.

The magnitude of the admixture is found to be $\sim 10^{-6} \times g_n^W$ that is an order of magnitude bigger than the PNC effects in normal spherical nuclei. What is important to notice is that the enhanced effect discussed here is proportional to the *neutron weak constant* g_n^W only. The value of this constant remains to be one of the most questionable points in modern theory of parity violation in nuclear forces [5]. The enhanced PNC mixing in halo found here can be therefore useful in studies of the neutron weak constant. Another interesting question related to the structure of the PNC force in nucleus, namely, the strength of the isovector P-odd potential that has been discussed in Refs. [6, 7].

7 Weak nucleon-nucleon interaction and parity violating effects. Potential approximation

We start with writing the nuclear Hamiltonian H in the form

$$H = H_S^0 + V_S^{res} + W^{PNC}, \quad (42)$$

where the first term $H_S^0 = \sum_a (\mathbf{p}_a^2/2m + U_S(\mathbf{r}_a))$ is the single particle Hamiltonian of the nucleons including the single-particle piece U_S of the strong interaction, V_S^{res} is the residual two-body strong interaction. The last term, W^{PNC} is the PNC part of the Weak interaction that is the source of the PNC effects.

The magnitude of the PNC effects is sensitive to both the weak PNC interaction matrix elements between the states of opposite parity and to the nuclear structure effects given by the strong part of the Hamiltonian 42. The latter one is invariant under spatial coordinate reflections, and if there is no weak interaction term W^{PNC} in 42, and as such parity is preserved, the eigenstates $|\Psi_s\rangle$ of the strong Hamiltonian $H_S^0 + V_S^{res}$ with energies E_s can be labeled by the parity quantum number (positive or negative), $|\Psi_s^+\rangle$, $|\Psi_s^-\rangle$. Due to presence of PNC weak interaction W^{PNC} in the nuclear Hamiltonian 42, a state of definite parity, say, $|\Psi_s^+\rangle$, acquires very small admixtures of wrong parity configurations. This can be accounted for by using the first order of perturbation theory with respect to W^{PNC} (see Eq. ??):

$$|\Psi_s^+\rangle' = |\Psi_s^+\rangle + \sum_{s_1} \frac{\langle \Psi_{s_1}^- | W^{PNC} | \Psi_s^+ \rangle}{E_s - E_{s_1}} |\Psi_{s_1}^-\rangle. \quad (43)$$

Here, prime denotes the corrected wave function that accounts for the PNC interaction and sum goes over available states of opposite parity, $|\Psi_{s_1}^-\rangle$. The magnitude of measurable PNC effects is normally proportional to the coefficients f^{PNC} [2] that determine the dominating admixtures of the wrong parity states

$$f = \frac{\langle \Psi_{s_1}^- | W^{PNC} | \Psi_s^+ \rangle}{\Delta E}. \quad (44)$$

The natural scale of the PNC effects in nuclei under usual conditions is [1],[2]

$$|f| \simeq 10^{-7} \quad (45)$$

that is roughly the ratio of the strength of the Weak PNC forces (matrix element in the numerator of 44) and the strength of the strong interaction (energy denominator in 44). In highly selective experiments, the PNC effects can be enhanced considerably as compared to estimate 45, due to specific properties of a specially chosen nuclear system or process. To reach high sensitivity to the wrong parity admixtures, one usually seeks possibilities to have the denominator ΔE in 44 minimal while keeping the PNC matrix element at maximum and to improve selectivity of measurable effect. This is typical for any tests of fundamental symmetries.

8 Microscopic PNC interaction

The most widely used version of the microscopic PNC interaction is the DDH Hamiltonian W_{DDH}^{PNC} [1], where the PNC forces are mediated by mesons. Its form stems from the analysis of interactions between intranucleon quarks via exchange of heavy bosons of Standard Model. The nonrelativistic P-odd weak interaction between nucleons approximated by the one-meson exchange can be written in the form [2, 1]

$$\begin{aligned}
W_{DDH}^{PNC} = & i \frac{h_\pi^{(1)} g_\pi}{4\sqrt{2}m} (\boldsymbol{\tau}_1 \times \boldsymbol{\tau}_2)^{(3)} (\boldsymbol{\sigma}_1 + \boldsymbol{\sigma}_2) \cdot [\mathbf{p}_1 - \mathbf{p}_2, \mathcal{F}_\pi] - \\
& - \frac{g_\rho h_\rho^0}{2m} (\boldsymbol{\tau}_1 \cdot \boldsymbol{\tau}_2) (\boldsymbol{\sigma}_1 - \boldsymbol{\sigma}_2) \cdot \{\mathbf{p}_1 - \mathbf{p}_2, \mathcal{F}_\rho\} - \\
& - \frac{g_\rho h_\rho^0}{2m} i(1 + \mu) (\boldsymbol{\tau}_1 \cdot \boldsymbol{\tau}_2) (\boldsymbol{\sigma}_1 \times \boldsymbol{\sigma}_2) \cdot [\mathbf{p}_1 - \mathbf{p}_2, \mathcal{F}_\rho] + W', \quad (46)
\end{aligned}$$

where the standard notations $F_{\pi(\rho)} = e^{-m_{\pi(\rho)}|\mathbf{r}_1 - \mathbf{r}_2|} / (4\pi|\mathbf{r}_1 - \mathbf{r}_2|)$ are used and $[\cdot, \cdot]$ and $\{\cdot, \cdot\}$ denote the commutator and anticommutator, respectively. The subscripts 1 and 2 label the interacting nucleons, the superscript (3) denotes the third isospin projection. Here, m , m_π and m_ρ are the masses of the nucleon, π - and ρ -meson, respectively; σ (τ) stand for the spin (isospin) Pauli matrices, $\mu = 3.7$ is the isovector part of the anomalous magnetic moment of nucleon. W' denotes contributions from heavier mesons, which are less important. The values of the corresponding weak and strong coupling constants $h_\pi^{(1)}$, g_π , g_ρ , and h_ρ^0 can be found in [1, 2].

9 Effects of the nuclear environment

In nuclear environment, a nucleon experiences the combined action of the PNC forces 46 from other nucleons. It is known, see, e.g., [2], that the most of P-odd effects caused by the weak interaction W_{DDH}^{PNC} , Eq. 46 in Eq. 42, can be successfully modeled by introducing the effective one-body P-odd interaction, or the “weak potential”, W_{sp} , acting on the nucleon 1 as a single-particle operator which arises from averaging W^{PNC} over the states of other nucleons $W_{sp} \equiv \langle W^{PNC} \rangle$. Within this approximation, the Hamiltonian of the weak interaction in a nucleus takes particularly simple form of a sum of the proton W_{sp}^p and neutron W_{sp}^n symmetry violating potentials

$$W_{sp} = W_{sp}^p + W_{sp}^n = g_p^W \frac{G}{2\sqrt{2}m} \{(\boldsymbol{\sigma}_p \cdot \mathbf{p}_p), \rho\} + g_n^W \frac{G}{2\sqrt{2}m} \{(\boldsymbol{\sigma}_n \cdot \mathbf{p}_n), \rho\}, \quad (47)$$

where $G = 10^{-5} m^{-2}$ is the Fermi constant, $\mathbf{p}_{p(n)}$ and $\boldsymbol{\sigma}_{p(n)}$ refer to the proton (neutron) momentum and doubled spin respectively. The coherent contribution from all the occupied nucleon orbitals composing the core yields the nuclear density $\rho = \sum_{occ} |\psi_{occ}|^2$ in the expression 47. The dimensionless constants g_p^W and g_n^W of order of unity, for the proton and neutron potentials, are related to the parameters of the DDH Hamiltonian and depend on nuclear charge and neutron number. The single-particle

approximation 47 for the PNC weak interaction 46 turns out to be very accurate [2]. It works satisfactorily even in the case of compound nuclear states [4, 26, 27, 28] where 47 gives the dominating contribution [26, 27] despite the fact that the wave functions are of essentially many-body nature.

9.1 Proton and neutron weak potential strengths

The knowledge about the proton and neutron constants g_p^W and g_n^W accumulated to date can be summarized as follows:

$$g_p^W = 4.5 \pm 2, \quad g_n^W = 1 \pm 1.5. \quad (48)$$

These widely used values [2, 5, 25, 26] correspond to the best values [1] of the microscopic parameters in the DDH Hamiltonian, Eq. 46, and they are found in reasonable agreement with the bulk experimental data on parity violation, including the compound nuclear experiments [3] and anapole moment measurements [32]. The above relatively small absolute value of the neutron constant that follows from DDH analysis, results basically from cancellation between π - and ρ -meson contributions to g_n^W , while both mesons contribute coherently to the proton constant g_p^W , see, e.g., [5]. Due to this difference between the absolute values of the proton and neutron constants, the proton constant tends to dominate most measurable PNC effects [24, 25, 29, 30], especially when both g_p^W and g_n^W can contribute. In some cases (such as odd proton nuclei), the contribution from the neutron constant, g_n^W , is suppressed irrespectively of its strength [2, 6]. In this sense, one usually measures the value of g_p^W , and it is difficult to probe g_n^W unless special suppression of the proton contribution occurs, and/or contribution of g_n^W is highlighted. By contrast, the case we consider in this work is sensitive to the value of the neutron constant only.

9.2 Halo structure effects on the PNC mixing

The basic specific properties of the halo nuclei are determined by the fact of existence of loosely bound nucleon in addition to the core composed by the rest of the nucleons [13] (we will be interested here in the most well studied case of neutron halo). The matter distribution is shown schematically in Fig. 4(I-a).

In one-body halo nuclei like ^{11}Be , the ground state is particularly simple: it can be represented as direct product of the single-particle wave function of the external neutron, ψ_{halo} , and the wave function of the core. The residual interaction V_S^{res} in Eq. 42 can be neglected as the many-body effects related to the core excitations are generically weak in such nuclei [34]. The problem with the Hamiltonian 42 is reduced to a single-particle problem for the external nucleon. The PNC potential matrix element between the ground state of halo nucleus and a state with opposite parity is

$$\langle \psi_{halo}^+ | W^{PNC} | \psi_{halo}^- \rangle = g_n^W \frac{G}{2\sqrt{2}m} \langle \psi_{halo}^+ | \{ (\boldsymbol{\sigma}_n \cdot \mathbf{p}_n), \rho_c \} | \psi_{halo}^- \rangle, \quad (49)$$

where $\rho_c(r)$ is the core density. Due to relatively heavy core for $A \simeq 10$, the difference between the center of mass coordinate and the center of core coordinate can also be neglected.

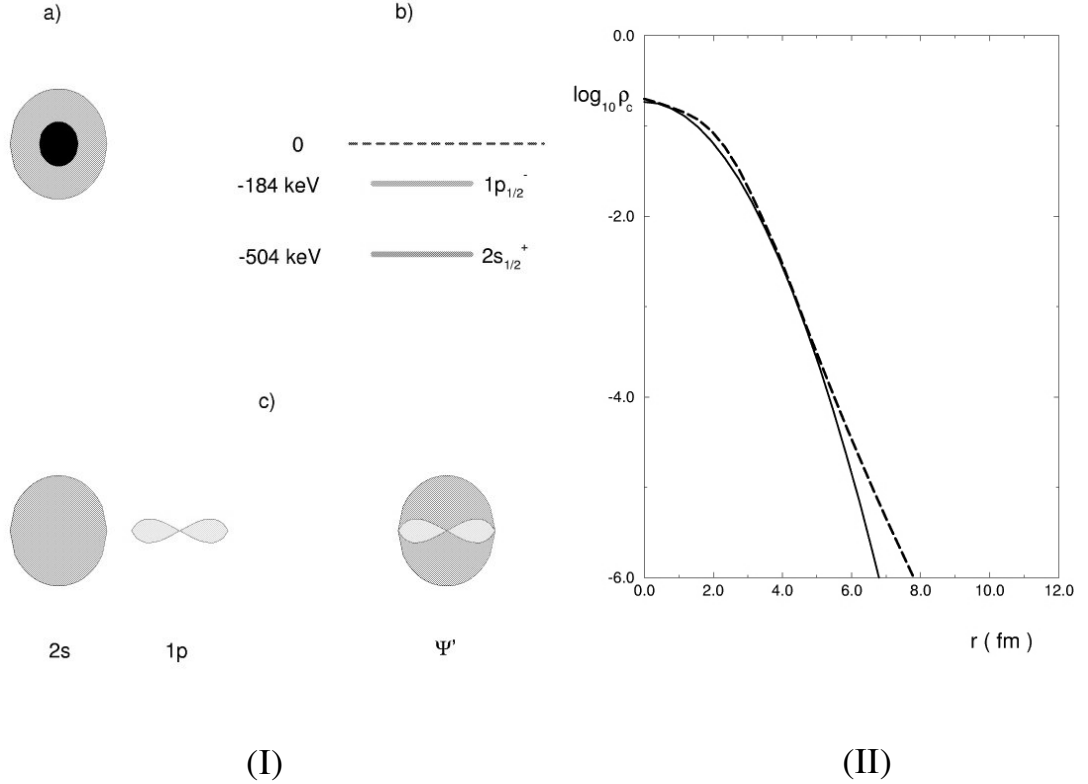


Figure 4 (I) a) Schematic plot of matter distribution in halo nuclei. The dark region corresponds to the nuclear core, the grey region shows the halo neutron cloud. b) The spectrum of the bound states ^{11}Be . c) Illustration of the single-particle PNC mixing in the ground state of ^{11}Be . (II) The core density distribution (logarithmic scale). The dashed line corresponds to Ref. [12], the solid line gives parametrization 56.

The effective potential that binds the external neutron is rather shallow yielding a small single-neutron separation energy, and one can expect small energy spacing between the opposite parity states. The PNC effects, Eqs. 44 and 43, can therefore be considerably magnified. The spectrum of ^{11}Be is shown in Fig. 4(I-b). To evaluate the PNC mixing f^{HALO} in the ground state of this nucleus, it is enough to know the single-particle matrix element between the ground state $2s$ and the nearest opposite parity state $1p$, and use their energy separation that is known experimentally.

The second effect of halo is that the value of the matrix element of the operator 47 between the halo states can be dramatically reduced as compared to its value in the case of “normal” nuclear states. The single-particle weak PNC potential 47 in Eq. 49 originates from the DDH Hamiltonian, Eq. 46, which is two-body operator, this fact is hidden in the nucleon density of the core $\rho_c(r)$. The external neutron spends most of its time away from the core region where only it can experience the PNC potential created by the rest of nucleons. Indeed, the dominant contribution to the matrix element of 47 between the halo states in 49 must come from the regions

where the three functions can overlap coherently: $\psi_{halo}^+(r)$, $\psi_{halo}^-(r)$ and the core density $\rho_{core}(r)$. The latter one is essentially restricted by the region of nuclear interior, $r < r_c$ thus reducing the effective volume of required interference region to $\frac{4}{3}\pi r_c^3$. Normalization condition implies that the extended wave function of the bound state halo $\psi_{halo}^\pm(r)$ must be considerably reduced in the volume of coherent overlap $\frac{4}{3}\pi r_c^3$. By contrast, in “normal” nuclei the radii of localization of the wave functions with opposite parity that can be mixed by the weak interaction coincide generically with the core radius r_c . The resulting suppression for the PNC halo matrix element $\langle \psi_{halo}^-(r) | W_{sp} | \psi_{halo}^+(r) \rangle$ with respect to the matrix element for the normal nuclei can be extracted from the following simple estimate

$$\frac{\langle \psi_{halo}^- | W_{sp} | \psi_{halo}^+ \rangle}{\langle \psi_{normal}^- | W_{sp} | \psi_{normal}^+ \rangle} \sim \left(\frac{r_c}{r_{halo}} \right)^3 \sim \left(\frac{2\text{fm}}{6\text{fm}} \right)^3 \sim \frac{1}{25} \dots \frac{1}{30} \quad (50)$$

where the mean square radii of halos from Ref. [12] was used. This suppression factor can cancel out the effect of the small energy separation (the denominator in Eq. 44) and to suppress the PNC effects. This simple estimate does not account for the structure of the halo wave functions which can be quite substantial and may even lead to further suppression in the PNC mixing. In the following, we present a detailed analysis of the related effects. The crude estimate 50 turns out rather pessimistic.

9.3 Halo model and evaluation of the PNC mixing in the ground state of ^{11}Be

The form of the single-particle wave functions of halo states can be deduced from their basic properties [16] and their quantum numbers [12]. The results of the Hartree-Fock calculations which reproduce the main halo properties (e.g., mean square radii) are also available [12]. One can use the following ansatz for the model wave function of the $2s$ halo state:

$$\psi_{2s} = R_{2s}(r) \Omega_{j=1/2,m}^{l=0}, \quad R_{2s}(r) = C_0 (1 - (r/a)^2) \exp(-r/r_0). \quad (51)$$

Here, $R_{2s}(r)$ is the radial part of the halo wave function and $\Omega_{j=1/2,m}^{l=0}$ is the spherical spinor. As we can neglect the center of mass effect for the heavy ($A = 10$) core, the halo neutron coordinate r in $R_{2s}(r) = \chi_{2s}(r)/r$ is reckoned from the center of nucleus. The constant C_0 is determined from the normalization condition, $\int_0^\infty dr [\chi_{2s}(r)]^2 = 1$ (the radial wave functions are chosen to be real). One has

$$C_0 = \frac{2^{3/2} a^2}{r_0^{3/2} \sqrt{45r_0^4 + 2a^4 - 12a^2 r_0^2}}. \quad (52)$$

The parameters r_0 and the a are the corresponding lengths to fit the density distributions obtained in Ref. [12] and the mean square radius. The value of a is practically fixed to be $a = 2\text{fm}$ what corresponds to the position of the node. The node position have been restored from the analysis of the scattering process [16].

For the wave function $\psi_{1p} = R_{1p}(r)\Omega_{j=1/2,m}^{l=1}$ of the excited state $1p$, the following simplest form of the radial wave function turns out to be adequate

$$R_{1p}(r) = C_1 r \exp(-r/r_1), \quad (53)$$

where C_1 is the normalization constant $C_1 = \frac{2}{\sqrt{3}}r_1^{-5/2}$ and the only tunable parameter r_1 is related to the $1p$ halo radius. The mean square root radii for the halo wave states, Eqs. 51 and 53, are given by

$$\sqrt{\langle r_{2s}^2 \rangle} = r_0 \left(\frac{6(45r_0^4 + 2a^4 - 12a^2r_0^2)}{105r_0^4 + a^4 - 15a^2r_0^2} \right)^{1/2}, \quad \sqrt{\langle r_{1p}^2 \rangle} = \left(\frac{15}{2} \right)^{1/2} r_1. \quad (54)$$

The matrix element of the weak interaction 47 and 49 between the ground state and the first excited state reads

$$\langle 2s | W_{sp} | 1p \rangle = ig_n^W \frac{G}{\sqrt{2m}} \int_0^\infty dr \chi_{2s}(r) \left(\rho_c(r) \frac{d}{dr} + \frac{\rho_c(r)}{r} + \frac{1}{2} \frac{d\rho_c(r)}{dr} \right) \chi_{1p}(r). \quad (55)$$

The core nucleon density $\rho_c(r)$ has been tuned to reproduce the data obtained from Ref. [12]. Their results are well reproduced by the Gaussian-shaped ansatz $\rho_c(r)$,

$$\rho_c(r) = \rho_0 e^{-(r/R_c)^2} \quad (56)$$

with the values of the parameters $\rho_0 = 0.2 \text{fm}^{-3}$ and $R_c = 2 \text{fm}$, as shown on Fig. 4(II).

Using the model wave functions 51 and 51 and the core density 56, the required integrals can be done analytically, and one arrives at the result

$$\langle 2s | W | 1p \rangle = ig_n^W \frac{G}{\sqrt{2m}} \mathcal{R} \quad (57)$$

where

$$\begin{aligned} \mathcal{R} = & \rho_0 R_c^3 C_0 C_1 \left\{ 3I_2(y) - \left[3 \left(\frac{R_c}{a} \right)^2 + 1 \right] I_4(y) + \right. \\ & \left. + \left(\frac{R_c}{a} \right)^2 I_6(y) - \frac{R_c}{r_1} \left[I_3(y) - \left(\frac{R_c}{a} \right)^2 I_5(y) \right] \right\} \end{aligned} \quad (58)$$

where $y = R_c(r_0 + r_1)/r_0 r_1$ and the functions I_n are given by

$$I_n(y) = \int_0^\infty dx \quad x^n e^{-x^2 - yx} = (-1)^n \frac{\sqrt{\pi}}{2} \frac{d^n}{dy^n} \left[e^{y^2/4} \text{erfc}(y/2) \right],$$

where $\text{erfc}(y)$ is the error function

$$\text{erfc}(y) = 1 - \frac{2}{\sqrt{\pi}} \int_0^y dt \quad \exp(-t^2/2).$$

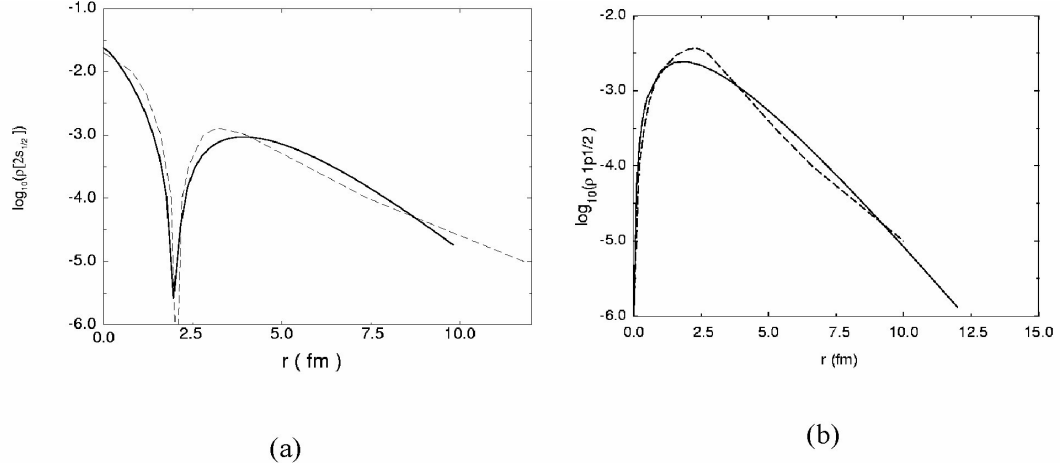


Figure 5 (a) The halo density in the ground state, $\rho_{2s1/2}(r) = (R_{2s1/2}(r))^2 / 4\pi$. The dashed line corresponds to the Hartree-Fock calculations of ref. [12], the solid line gives parametrization 51. (b) The halo density in the first excited state, $\rho_{1p1/2}(r) = \frac{1}{4\pi} (R_{1p1/2}(r))^2$. The dashed line corresponds to the Hartree-Fock calculations of Ref. [12], the solid line gives parametrization 53 and 59.

To obtain the results for the PNC weak interaction matrix element, one can use the parameters r_0 and r_1 in the halo wave functions to fit the radial densities of the halos obtained by H. Sagawa [12].

The results for the best parameters are shown in Figs. 5(a) and 5(b) for the $2s$ and the $1p$ halos, respectively. One sees that the agreement for the densities is good. Below, the values

$$r_0(\text{best value}) = 1.45\text{fm}, \quad r_1(\text{best value}) = 1.80\text{fm}, \quad (59)$$

are used to calculate the matrix elements in Eqs. (55, 57 and 58). The radial wave functions χ are given in Fig. 6(a). To check robustness of the results with respect to variations in the halo structure details, deviations of the both r_0 and r_1 from 59 were used. The values of the halo radii given by 54, $\sqrt{\langle r_{2s}^2 \rangle} = 5.9\text{fm}$ and $\sqrt{\langle r_{1p}^2 \rangle} = 4.9\text{fm}$ are close to the values of ref. [12] 6.5fm and 5.9fm which agree with experimental matter radii.

Substituting the values 59 into the expressions for the matrix elements one obtains the following value of the matrix element $\langle 2s | W_{sp} | 1p \rangle_{HALO}$

$$\begin{aligned} \langle 1p | W_{sp} | 2s \rangle_{HALO} &= -i 0.2 g_n^W \text{ eV}, \\ &= -i 0.2 \text{ eV} \quad (\text{for } g_n^W \simeq 1). \end{aligned} \quad (60)$$

It is seen that this value is only few times smaller than the standard value of the matrix element of the weak potential between the opposite parity states in spherical nuclei (see e.g., Ref. [2]), that is typically about one eV . This results from the

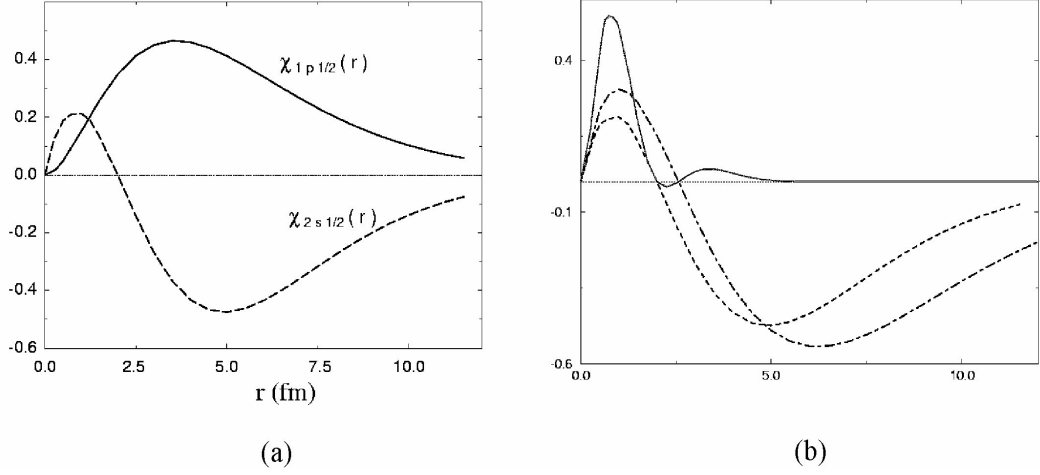


Figure 6 (a) Plot of the radial wave functions of the states $|2s1/2\rangle$ and $|1p1/2\rangle$, $\chi_{2s1/2}(r) = rR_{2s1/2}(r)$ and $\chi_{1p1/2}(r) = rR_{1p1/2}(r)$. (b) Plot of the functions contributing to the weak PNC matrix element. The function $s(r) = \frac{d}{dr}\chi_{1p1/2}(r) + \frac{\chi_{1p1/2}(r)}{r} + \frac{d\rho_c/dr}{2\rho_c}\chi_{1p1/2}(r)$ (dot-dashed line) depends on r in the way similar to $\chi_{2s1/2}(r)$ (dashed line). The combination $\chi_{2s1/2}(r)\rho_c s(r)$ that enters the PNC matrix element in Eq.(55) is shown by the solid line. It contributes coherently to $\langle 2s|W_{sp}|1p\rangle$.

wave function structure and comes basically from the facts that the $2s$ wave function crosses zero line near the core surface while the $1p$ radial wave function does not have nodes. Thus the functions χ_{1p} and $d\chi_{2s}/dr$ look similar and are folded constructively with $\rho_c(r)$ in the region of interaction (nuclear interior), see Fig. 6(b).

The matrix element of W_{sp} between the “normal” nuclear states can be evaluated for example, in the oscillator model. Taking the typical matrix element between the states $2s$ and $1p$ and using the same formula 55, one has

$$\langle 1p|W_{sp}|2s\rangle_{osc} = -ig_n^W G\rho_0 \left(\frac{\omega}{2m}\right)^{1/2} \quad (61)$$

where $\omega \simeq 40A^{-1/3}\text{MeV}$ is the oscillator frequency [33] with A the nuclear mass number. We used here the constant value of the core nucleon density, $\rho_0 \simeq 0.138\text{fm}^{-1/3}$. This is a good approximation in the case of normal nuclei [26].

Recalling the energy difference between the ground state and the first excited state $1p$ that is known experimentally,

$$|\Delta E_{HALO}| = E_{p1/2} - E_{s1/2} = 0.32\text{MeV} \quad (62)$$

we obtain, using Eq. 60, the coefficient of mixing the opposite parity state ($1p$) to the halo ground state $2s$:

$$\begin{aligned} |f_{sp}^{HALO}| &= \frac{|\langle 1p|W_{sp}|2s\rangle|}{|\Delta E_{HALO}|} \simeq \frac{0.2eVg_n^W}{0.32\text{MeV}} \\ &\simeq 0.6 \times 10^{-6} g_n^W \simeq 0.6 \times 10^{-6} \quad (\text{for } g_n^W \simeq 1). \end{aligned} \quad (63)$$

This PNC mixing is about one order of magnitude stronger than the scale of single-particle PNC mixing in “normal” nuclear states that can be extracted from Eq. 61. In the case of normal $p - s$ mixing, we have

$$\begin{aligned} |f_{sp}^{normal}| &= \frac{|\langle 1p|W_{sp}|2s\rangle|}{\omega} = \frac{Gg_n^W \rho_0}{\sqrt{2}m} \left(\frac{m}{\omega}\right)^{1/2} \\ &\simeq 0.7 \times 10^{-7} g_n^W \simeq 0.7 \times 10^{-7} \quad (\text{for } g_n^W \simeq 1) \end{aligned} \quad (64)$$

in the same region of nuclei with $A \sim 11$. The above value 64 for the normal PNC mixing is rather universal and it is practically insensitive to variations of the details of the normal nuclear wave functions and core densities [26]. One should stress that in the halo case, the energy denominator in Eq. 63 is $\omega/|\Delta E_{HALO}| \simeq 50$ times smaller than in the normal case 64, based on the oscillator model. Comparing Eqs. 63 and 64, we find the halo enhancement factor in the PNC mixing to be

$$\frac{|f_{sp}^{HALO}|}{|f_{sp}^{normal}|} \simeq 9.$$

This result is quite remarkable in a number of respects. First, it is seen that in experiments when the halo wave functions in nuclear exterior are probed, the value of PNC mixing is even stronger than in “normal” nuclei. Secondly, this PNC mixing is dominated by the neutron weak constant g_n^W . Such experiments with neutron halo nuclei therefore provides a unique opportunity to probe the value of this constant. Usually, the sensitivity of experiments to the value of this constant is “spoiled” by comparably large value of the proton weak constant g_p^W , cf. Eq. 48.

In order to assess the reliability of these results, one can verify the stability of the enhancement factor against variations in the parameters of the halo wave functions. As one can see from the results presented in Table 10.1, the matrix element 60 is changed by few per cent only when the wave functions are deformed. The enhancement factor 63 is therefore quite stable.

	$r_0 = 1.40$	$r_0 = 1.45$	$r_0 = 1.50$
$r_1 = 1.75$	1.168	1.052	0.950
$r_1 = 1.80$	1.110	1.000	0.903
$r_1 = 1.85$	1.056	0.952	0.860

Table 10.1 - Stability analysis for the matrix element of W_{sp} between the halo states $2s_{1/2}$ and $1p_{1/2}$. The results for the values of the parameters r_0 and r_1 differing from the best values are shown. The central entry in the table corresponds to the best value. It is seen that variations in r_0 and r_1 do not affect $\langle 2s_{1/2}|W_{sp}|1p_{1/2}\rangle$ any considerably.

The analysis presented above rests basically on the most reliably known facts: the quantum numbers of the states involved, the halo radii which match the matter radii known from experiment, and the Hartree-Fock wave functions. With these input data, the further quantitative analysis is a straightforward analytical exercise which does not require any approximations. The stability of the results has been checked

analytically. The PNC enhancement factor of one order of magnitude allows one to speak about qualitative halo effect that should not be overlooked.

It is the matter of further studies to check the universality of the effect while going along the table of exotic nuclei. One sees that other exotic nuclei with developed halo structure manifest similar properties (see, e.g., [12]). Indeed, the effect of PNC enhancement shown here results basically from the two facts:

- (i) small energy separation between the mixed opposite parity states
- (ii) considerably strong overlap between the mixed wave functions and the core density, which saves part of suppression in the PNC weak matrix element.

The first of these points is rather common for nuclei with developed neutron halos. Systematics of separation energies for single neutron [13] shows that the ground states of halo nuclei can be distanced from the continuum by typical spacing $\varepsilon_{halo} \sim (2mr_{halo})^{-1/2} \sim$ few hundreds of keV. Even in the cases when no bound states with parity opposite to that of the ground state occur, the PNC admixtures to the ground state wave functions must exist. In these cases, the PNC admixtures can be evaluated by means of Green function method.

The second point (ii) is related to the wave function structure. It would be also interesting to study the PNC effects in proton rich nuclei [20, 21, 22].

The results shown here are based on the single-particle approximation (one-body halo model). In principle, the halo neutron can couple to excitations of the core (see, e.g., Ref. [34]). In fact, such coupling can be responsible for the small energy separation between the opposite parity levels in ^{11}Be , which can be separated by few MeV otherwise (see, e.g., [23]). These many-body effects may be important for precise evaluation of the PNC mixing. We did not consider contribution from such effects here.

One of possible experimental manifestations of the discussed effect is related to anapole moment (discussed in the next Section) [24, 25] which attracts much attention in current literature [31] in view of new experimental results (detection of anapole moment in the nucleus ^{133}Cs [32]). Since the anapole moment is created by the toroidal electromagnetic currents which results from PNC, its value grows as the size of the system increased [25]. In the case of halo which we considered here, the value of the anapole moment can be therefore enhanced due to extended halo cloud. We will discuss this feature in the next Section.

10 Anapole moment of an exotic nucleus

The nuclear anapole moment is one of the most interesting manifestations [24, 25, 35, 29, 30, 36, 37, 31, 32] of the spatial Parity Nonconservation (PNC) [1, 2] in atomic physics. It arises from the PNC nuclear forces which create anomalous (toroidal) contributions to the electromagnetic current. The resulting PNC magnetic field can be experienced by an external lepton (e.g., atomic electron or muon in mesic atom) and can be detected in hyperfine structure atomic measurements. The effect of the anapole moment, which depends on the nuclear spin, can be experimentally separated from other PNC contributions [37, 31, 32]. Few theoretical papers have been devoted to the problem of nuclear anapole moments [25, 35, 29, 30, 36]. The first calculation

of the quantity in the single-particle approximation has been done by Flambaum and Khriplovich [25]. Calculation of the anapole moment with accounting for residual pion-mediated interaction has been made by Haxton, Henley, and Musolf [29], where an expression for the anapole moment operator has been derived, which preserves the gauge invariance automatically. In Ref. [36] various many-body corrections to the anapole moments (basically, the many-body contributions to the current) have been taken into account. This field attracts much attention [36, 37, 31, 32, 7] as some experimental results for the nuclear anapole in Cs are available [37, 32].

The studies of the anapole moment have been mostly confined to the case of normal nuclei. Specific structure of exotic nuclei [11, 12, 13, 15, 16, 20, 21, 22, 34, 38, 39, 40, 41] can offer new possibilities to probe those aspects of nuclear interactions which are not accessible with normal nuclei. The problem of the PNC effects in exotic nuclei has been addressed in the last sections [19] where it was shown that the PNC mixing in halo nuclei can be considerably enhanced as compared to the case of normal nuclei. It is therefore interesting to examine the anapole moments of the exotic nuclei.

Let us estimate the anapole moment of an exotic halo nucleus, focusing on the case of ^{11}Be which has been extensively studied both experimentally and theoretically [11, 12, 13, 15, 16]. We call the resulting anapole moment “anomalous” as it exceeds by fifteen times the average anapole moment of a normal nucleus of the same mass and is bigger than the anapole moment of any known neutron-odd nucleus. The value of the anapole moment is even twice bigger than that of lead.

Supplement B

11 Nuclear spin dependent PNC interaction of a lepton with nucleus via the anapole moment

The part of the Hamiltonian of the nucleus-lepton system in which we are interested in can be written in the form

$$H = H_0^n + V_{res}^n + W_{PNC}^n + H_{PNC}^{n-e} + h_{PNC}^{n-e}, \quad (65)$$

where $H_0^n = \sum_i [\mathbf{p}_i^2/2m + U_S(\mathbf{r}_i)]$ is the single particle Hamiltonian of the nucleons with momentum \mathbf{p} and mass m in the single-particle potential $U_S(r)$; V_{res}^n is the residual strong interaction. The operator W_{PNC}^n is the weak PNC nucleon-nucleon interaction [1]. The term H_{PNC}^{n-e} describes the interaction of the lepton with the vector potential \mathbf{A}_{PNC} created by the nucleus, in which we save only the PNC part,

$$H_{PNC}^{n-e} = e(\boldsymbol{\alpha} \cdot \mathbf{A}_{PNC}) = e(\boldsymbol{\alpha} \cdot \langle \mathbf{a} \rangle) \Delta(\mathbf{r}) \quad (66)$$

where $\boldsymbol{\alpha}$ denote the Dirac matrices [33] for the lepton and $\Delta(r)$ is a function sharply peaked in the region of the nucleus (it reduces to the δ -function on the scale of the atomic electron spatial motion), e is the proton charge, $e^2 = 1/137$. The last term, h_{PNC}^{n-e} , is the part of the neutral current interaction contributing to the PNC nucleus-lepton forces depending on nuclear spin,

$$h_{PNC}^{n-e} = \kappa_{nc} \frac{G}{\sqrt{2}} \frac{[1/2 - (-1)^{j+l+1/2}(j+1/2)]}{j(j+1)} (\mathbf{j} \cdot \boldsymbol{\alpha}) \Delta(\mathbf{r}), \quad (67)$$

where $\kappa_{nc} \equiv (5/8)(1 - 4 \sin^2 \theta)$ with θ the Weinberg angle.

The vector $\langle \mathbf{a} \rangle$ is the expectation value of the anapole moment operator

$$\mathbf{a} = -\pi \int d^3r r^2 \mathbf{J} \quad (68)$$

in the nuclear ground state, where J is the nuclear electromagnetic current. Its is convenient to define the ‘‘anapole moment’’, κ , rewriting Eq. 66 according to [35]

$$H_{PNC}^{n-e} = e(\boldsymbol{\alpha} \cdot \langle \mathbf{a} \rangle) \Delta(\mathbf{r}) \equiv \kappa \frac{G}{\sqrt{2}} \frac{(-1)^{j+l+1/2}(j+1/2)}{j(j+1)} (\mathbf{j} \cdot \boldsymbol{\alpha}) \Delta(\mathbf{r}), \quad (69)$$

where j is the nuclear spin in the ground state which coincides with the angular momentum of the external nucleon if one works in the single-particle approximation; where $G = 10^{-5} m^{-2}$ is the Fermi constant and m is the nucleon mass. The factors depending on j and on the orbital angular l of the external nucleon absorb the spin-angular dependence of the anapole expectation value $\langle a \rangle$, and the anapole moment κ chosen in this way contains merely the nuclear structure information.

In the single-particle approximation, the most important part of the anapole moment operator 68 can be written [35, 29] as the sum of the spin-current term and an additional term δa

$$\mathbf{a} = \frac{\pi e}{m} \sum_i \mu_i (\mathbf{r}_i \times \boldsymbol{\sigma}_i) + \delta \mathbf{a}, \quad (70)$$

which includes other contributions. Here, σ are the spin Pauli matrices, μ are the nucleon magnetic moments (+2.79 for proton and -1.91 for neutron). The last term in Eq. 70 abbreviates contribution from the orbital current and the corrections which come basically from the interaction many-body contributions (e.g., from the weak forces) to the electromagnetic current [25, 29, 36]. They are proportional to the charge of the external nucleon, and in our case (external neutron) the first term in Eq. 70 dominates in the single-particle approximation.

The expectation value of 70 in any eigenstate of the nuclear Hamiltonian, $H_0^n + V_{res}^n$ is zero unless parity violating forces W_{PNC}^n are taken into account. As a result of the PNC weak interaction W_{PNC}^n in the Hamiltonian 65, a nuclear state of definite parity $|\psi\rangle$, acquires very small admixtures of wrong parity configurations $|\bar{\psi}_n\rangle$. This can be accounted for by using the first order of perturbation theory with respect to W_{PNC}^n . Thus the expectation value of the anapole moment operator \mathbf{a} in the state $|\tilde{\psi}\rangle$ with energy E containing the PNC admixtures is

$$\langle \tilde{\psi} | \mathbf{a} | \tilde{\psi} \rangle = \sum_n \left(\frac{\langle \psi | W_{PNC} | \bar{\psi}_n \rangle \langle \bar{\psi}_n | \mathbf{a} | \psi \rangle - \langle \psi | \mathbf{a} | \bar{\psi}_n \rangle \langle \bar{\psi}_n | W_{PNC} | \psi \rangle}{E - E_n} \right) \quad (71)$$

where sum runs over the opposite parity states $|\bar{\psi}_n\rangle$. In a finite nucleus, a nucleon experiences the combined action of the two-body PNC forces W_{PNC} [1] from other nucleons, which can be modeled [2] by the effective one-body PNC weak potential w_{PNC} (see Eq. 49)

$$w_{PNC} = g \frac{G}{2\sqrt{2}m} \{(\boldsymbol{\sigma} \cdot \mathbf{p}), \rho\},$$

where the curly brackets denote anticommutator. The nuclear core density $\rho = \sum_{occ} |\psi_{occ}|^2$ in 47 reflects the coherent contribution from all the occupied nucleon orbitals. The dimensionless constants g for proton and neutron are $g_p = 4.5 \pm 2$, $g_n = 1 \pm 1.5$. These widely used values [2, 25, 35, 26] correspond to the best values [1] of the microscopic parameters in the DDH Hamiltonian [1]. They are found in reasonable agreement with the bulk experimental data on PNC including the compound nuclear experiments by TRIPLE group [3] and anapole moments of stable nuclei [32].

12 Weak interaction and the anapole moment in halo nucleus

The basic specific properties of the halo nuclei are determined by the fact of existence of loosely bound nucleon in addition to the core composed by the rest of the nucleons [13].

In one-body halo nuclei like ^{11}Be , the ground state is particularly simple: it can be represented as direct product of the single-particle wave function of the

external neutron, ψ_{halo} , and the wave function of the core. The spin-saturated core does not contribute to 71. The residual interaction V_{res}^n in Eq. 65 can be neglected as the many-body effects related to the core excitations are generically weak in such nuclei [34]. As a result of the relatively heavy core for $A \simeq 10$, difference between the center of mass coordinate and the center of core coordinate can also be neglected. The problem with the Hamiltonian 65 and 47 is reduced to a single-particle problem for the external nucleon. For the nucleus with the external *neutron*, as is the case for the halo nucleus ^{11}Be , the orbital part of the anapole operator 70 does not contribute. Using the reduced matrix elements of the spin-angular part of the operator 70,

$$\langle l', j, m | \frac{\mathbf{r}}{r} \times \boldsymbol{\sigma} | l, j, m \rangle = i(-1)^{j+l+1/2}(j+1/2)\sqrt{\frac{2j+1}{j(j+1)}}, \quad l' = l \pm 1,$$

the anapole moment can be expressed in terms of the radial wave functions R_{nlj} as follows:

$$\begin{aligned} \kappa = & -\frac{2\pi\mu_n e^2 g_n}{m^2} \sum_{n'l'j} \int_0^\infty r^2 dr R_{n'l'j} [\rho(dR_{nlj}/dr + (l-j)(2l+1-j)R_{nlj}/r) \\ & + (d\rho/2dr) R_{nlj}] \int_0^\infty r^3 dr R_{n'l'j} R_{nlj} / (E_{nlj} - E_{n'l'j}). \end{aligned} \quad (72)$$

In a halo nucleus like ^{11}Be or ^{11}Li , the energy spacing between the opposite parity weakly-bound states can be small [11, 12, 13, 15, 16, 34]. The PNC effect in 72 can therefore be considerably magnified [19]. The nucleus ^{11}Be has the only bound excited state, $1p_{1/2}$, above the ground state $2s_{1/2}$ [11, 12, 15, 16] (inversion of levels). As a result of the small energy separation between these levels of opposite parities which is known experimentally, Eq. 62, one can save the only $1p_{1/2}$ term in the expression 72 for the anapole moment κ of the ground state $2s_{1/2}$. The form of the single-particle wave functions of halo states can be deduced from their basic properties [16] and their quantum numbers [12]. The results of the Hartree-Fock calculations which reproduce the main halo properties (e.g., mean square radii) are also available [12]. We use the following ansatz [19, 9] for the model wave functions of the $2s$ and the excited $1p$ halo states as given by Eq. 51. The core nucleon density $\rho_c(r)$ has been taken according to Eq. 56, as shown on Fig. 7(a). Evaluation of Eq. 72 with the wave functions 51 and the core density 56 gives the expression for the anapole moment in terms of the parameters of Eq. 57.

The results for the densities are shown in Fig.7(a). One sees good agreement with the Hartree-Fock calculations [12]. The values of the halo radii given by 54, $\sqrt{\langle r_{2s}^2 \rangle} = 5.9$ fm and $\sqrt{\langle r_{1p}^2 \rangle} = 4.9$ fm are close to the values of Ref.[12] 6.5 fm and 5.9 fm which agree with experimental matter radii.

With the above values of the parameters, one obtains from 72 the resulting value of the anapole moment κ

$$\kappa(^{11}\text{Be}) = 0.17g_n = 0.17 \quad (\text{for } g_n \simeq 1). \quad (73)$$

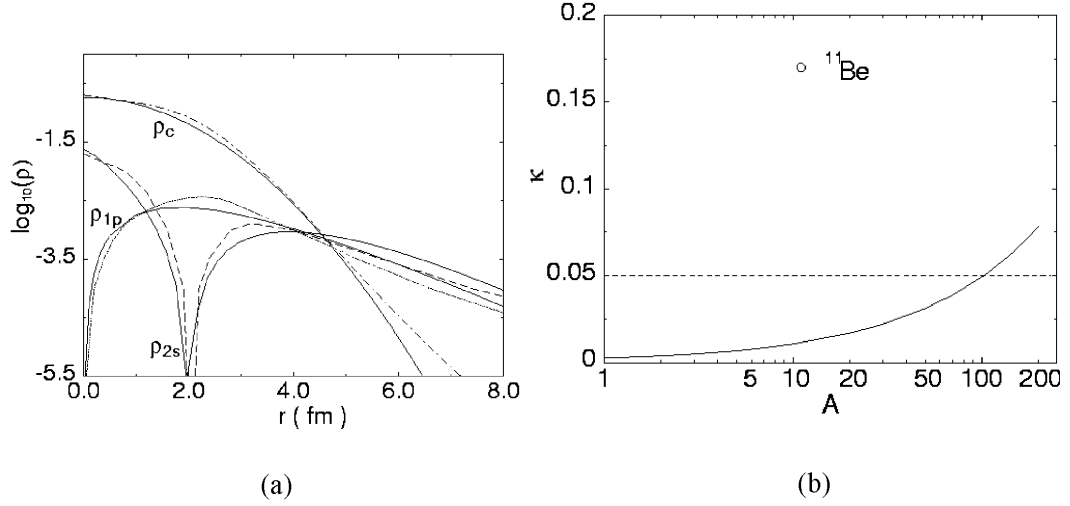


Figure 7 (a) Densities $R^2(r)$ for the halo states $2s$ and $1p$ as function of r and the core density $\rho_c(r)$ calculated from Eqs. (51,56) (solid lines). The Hartree-Fock results for the same quantities [12] are given by the dashed line, the dotted line and the dotted-dashed line, respectively. (b) “Halo anomaly” in ^{11}Be : the value $\kappa(^{11}\text{Be})$ (circle) as compared to the absolute values of the anapole moments of normal neutron-odd nuclei (solid curve) and the neutral current contribution $\kappa_{nc} = 0.05$ (dashed curve).

It is few times bigger than the contribution from neutral current $-\kappa_{nc} = -0.05$. Thus the nuclear spin-dependent PNC interaction of a lepton with the halo nucleus is dominated by the anapole moment contribution, as in heavy nuclei.

To appreciate how big the value $\kappa(^{11}\text{Be})$ is, one can compare 73 to the anapole moment of the normal spherical nucleus with odd neutron which is given by [35]:

$$\kappa_{norm} = \frac{9}{10} \frac{g_n e^2 \mu_n}{m r_0} A^{2/3}, \quad (74)$$

where $r_0 = 1.2$ fm is the nucleon radius. Resulting from the PNC toroidal electromagnetic currents, the anapole moment grows fast ($\propto A^{2/3}$) as the size of the system increases [25, 35]. For this reason, the anapole moments of *normal* light nuclei give only a small correction to the neutral current lepton-nucleus PNC interaction (see Fig. 7(b)). From 73 and 74, we find the ratio of the anapole moment to its value in a nucleus with the same A (enhancement factor):

$$R_{halo} = \frac{\kappa(^{11}\text{Be})}{\kappa_{norm}} = 15. \quad (75)$$

In fact, the anapole moment 73 exceeds few times the anapole moments of any known odd nucleus, as seen in Fig.7(a). For example, the $\kappa(^{11}\text{Be})$ is two times bigger than the anapole moment of nucleus as heavy as lead [35],

$$\kappa(^{207}\text{Pb}) = -0.08g_n.$$

The remarkable enhancement factor 75 in 73 comes from the two features of the halo structure: a) enhancement of the PNC mixing in the halo ground state [the first factor in Eq. 76] and b) enhancement of the matrix elements of the anapole operator in halo states:

$$R_{halo} \sim \frac{\omega}{\Delta E} \left(\frac{w_{halo}}{w_{norm}} \right) \left(\frac{r_{halo}}{r_{norm}} \right), \quad (76)$$

where the second factor is the ratio of the halo weak matrix element w_{halo} , Eq. 47, to the normal one, w_{norm} , which is less than unity. The parity violating effect originates from the weak interaction of the external halo neutron with the core nucleons in the nuclear interior. As a result, the neutron halo cloud surrounding the nucleus acquires the wrong parity admixtures. Those give rise to the PNC toroidal currents in the nuclear exterior (the halo region) which results in additional enhancement of the anapole moment [the last factor in 76].

13 Many-body corrections to the anapole moment

We discuss now the stability of the results against possible distortions of the wave functions 51. Table 10.2 shows the values of the anapole moment calculated for various values of the parameters r_0 and r_1 in the wave functions 51. As is seen from the Table, the results are stable with respect to variation of the details of the halo structure.

	$r_0 = 1.35$	$r_0 = 1.40$	$r_0 = 1.45$	$r_0 = 1.50$	$r_0 = 1.55$
$r_1 = 1.70$	1.26	1.15	1.05	0.96	0.87
$r_1 = 1.75$	1.23	1.12	1.03	0.94	0.85
$r_1 = 1.80$	1.19	1.09	1.00	0.91	0.83
$r_1 = 1.85$	1.16	1.06	0.97	0.89	0.81
$r_1 = 1.90$	1.12	1.03	0.95	0.87	0.80

Table 10.2 - Dependence of κ (^{11}Be) on the halo parameters r_0 and r_1 in Eq.57; the ratios of κ to the result 60 are given. The central entry in the table corresponds to the optimal values used in 60. It is seen that variations in r_0 and r_1 do not appreciably affect 60.

We consider now the influence of possible many-body contributions (see, e.g., [39, 40]) to the halo wave functions 51 on the present results based on single-particle picture.

The generalized wave function of the halo ground state, $|s\rangle$, can be written as a sum

$$|s\rangle = (1 - x_s^2)|s_{sp}\rangle + x_s|S_{mb}\rangle,$$

where $|s_{sp}\rangle$ is the purely single-particle s-state in Eqs. 71 and 51, and $|S_{mb}\rangle$ denotes the many-body contributions due to core polarization, deformations *etc.*, which have not been considered yet. The coefficient x_s ($0 \leq x_s \leq 1$) is the amplitude of the many-body contribution which is assumed to be properly normalized, $\langle S_{mb}|S_{mb}\rangle = 1$. The

anapole moment can be evaluated in the same way as above, using Eqs. 70, 71 and 47 and substituting the state $|s\rangle$ instead of $|s_{sp}\rangle$. Both the anapole moment operator 70, the weak potential 47 are the single-particle operators, so they can not connect the single-particle wave function $|p_{sp}\rangle$ 51 with the many-body component $|S_{mb}\rangle$. Thus

$$\langle S_{mb}|\mathbf{a}|p_{sp}\rangle = 0 \quad \text{and} \quad \langle S_{mb}|w_{PNC}|p_{sp}\rangle = 0. \quad (77)$$

The anapole moment $\tilde{\kappa}$ in the state $|s\rangle$ is now given by the simple renormalization of the result obtained above,

$$\tilde{\kappa} = (1 - x_s^2)\kappa,$$

where κ is the single-particle result 72, 57 and 73. Similarly to Eq. 77, one can take into account many-body contributions $|P_{mb}\rangle$ to the excited p-state $|p_{sp}\rangle$ (51) with the amplitude x_p , $|p\rangle = (1 - x_p^2)|p_{sp}\rangle + x_p|P_{mb}\rangle$. In this case, the modified result for the anapole moment is:

$$\tilde{\kappa} = \kappa \left[(1 - x_s^2)(1 - x_p^2) + x_s x_p \sqrt{(1 - x_s^2)(1 - x_p^2)(u + v) + x_s x_p uv} \right], \quad (78)$$

where $u = \langle S_{mb}|\mathbf{a}|P_{mb}\rangle / \langle s_{mb}|\mathbf{a}|p_{mb}\rangle$ and $v = \langle S_{mb}|w_{PNC}|P_{mb}\rangle / \langle s_{mb}|w_{PNC}|p_{mb}\rangle$ denote the ratios of the matrix elements of the anapole (weak interaction) between the many-body components S_{mb} and P_{mb} to their values for the single-particle states. One can note that the matrix elements of the single-particle operators between the many-body wave functions are generically suppressed as compared to those between the single-particle states, so that the factors u and v can be neglected for the sake of estimate.

According to experimental results [41], the many-body contributions to the halo ground state in ^{11}Be are rather small, $\approx 16\%$. Assuming the many-body corrections to the excited states of the same magnitude, $x_p \simeq x_s$, one can conclude from Eq. 78 that the results obtained in the single-particle approximation could hardly be reduced by more than 30 per cent.

The corrections due to the many-body admixtures in the halo states are therefore about the same order of magnitude as the many-body corrections to the operators 70 and 47. They can be taken into account in more refined calculations using detailed information on the wave function structure.

The curious ‘‘halo anomaly’’ illustrated in Fig. 7(b) can be quite interesting in a number of respects. First, the search for sources of enhancement in anapole moments has been always important from the experimental viewpoint. Possibilities offered by the normal nuclei are rather limited here. The most promising case of deformed nuclei, where one can find close levels of opposite parity near the ground state, does not offer any enhancement because of the suppression in the matrix elements of \mathbf{a} [35]. In this respect, the anomalies in anapole moments of exotic nuclei like ^{11}Be seem to give unexpected opportunity. Secondly, the anapole moment of neutron-rich nuclei is determined by the neutron weak constant g_n only. Usually, the sensitivity of experiments to the value of this constant is ‘‘spoiled’’ by relatively large value of the proton weak constant g_p , in Eq.47. The large enhancement of the anapole moment

in neutron halo nuclei provides therefore an unique opportunity to test the isospin structure of the weak potential 47 which is of great interest [7].

One should note that the nucleus ^{11}Be has a rather long life-time (13.81 sec). This makes therefore possible, at least in principle, the atomic measurements of the hyperfine structure effects in traps planned for the ISOL facility where the anapole moment can be detected.

It would be also interesting to consider mesic atoms with exotic nuclei, where the effect can be further enhanced, as the heavy lepton orbits are closer to nucleus than in usual atoms. The case of proton rich nuclei where the effect must be more pronounced due to numerical value of the constant g_p , is also of separate interest.

14 References

1. B. Desplanques, J. Donoghue, and B. Holstein, Ann. Phys. (N.Y.) **124** (1980) 449
2. E.G. Adelberger and W.C. Haxton, Ann. Rev. Nucl. Part. Sci. **35** (1985) 501.
3. J.D. Bowman, C.D. Bowman, J.E. Bush, P.P.J. Delheij, C.M. Frankle, C.R. Gould, D.G. Haase, J. Knudson, G.E. Mitchel, S. Penttila, H. Postma, N.R. Robertson, S.J. Seestrom, J.J. Szymansky, V.W. Yuan, and X. Zhu, Phys.Rev.Lett. **65** (1990) 1192.
4. M.B. Johnson, J.D. Bowman, and S.H.Yoo, Phys. Rev. Lett. **67** (1991) 310.
5. O.P. Sushkov and V.B. Telitsin, Phys. Rev. **C48** (1993) 1069.
6. B. Desplanques, Phys. Rep. **297** (1998) 1.
7. W.S. Wilburn and J.D. Bowman, Phys. Rev. **C57** (1998) 3425.
8. D.B. Kaplan, M.J. Savage, R.P. Springer, and M.B. Wise, Phys. Lett. **B449** (1999) 1.
9. H. Feshbach, M.S. Hussein, A.K. Kerman, and O.K.Vorov, Adv. Nucl. Phys. **25**
10. J.S. Al-Khalili and J.A. Tostevin, Phys. Rev. Lett. **76** (1996) 3903.
11. R.C. Johnson, J.S. Al-Khalili, and J.A. Tostevin, Phys. Rev. Lett. **79** (1997) 2771.
12. H. Sagawa, Phys. Lett. **B286** (1992) 7.
13. C.A. Bertulani, L.F. Canto, and M.S. Hussein, Phys. Rep. **226** (1993) 281.
14. C.A. Bertulani, L.F. Canto, and M.S. Hussein, Phys. Lett. **B353** (1995) 413.
15. K. Hencken, G. Bertsch and H. Esbensen Phys. Rev **C54** (1996) 3043.
16. A. Mengoni, T. Otsuka, T. Nakamura, and M. Ishihara, Contribution to the 4th International Seminar on Interaction of Neutrons with Nuclei, Dubna (Russia), April 1996, Preprint nucl-th/9607023.
17. J. Hardy, In *Physics of Unstable Nuclear Beams*, C.A.Bertulani, L.F.Canto, and M.S.Hussein ed., World Scientific, Singapore, 1997.
18. T. Suzuki, In *Physics of Unstable Nuclear Beams*, C.A.Bertulani, L.F.Canto, and M.S.Hussein ed., World Scientific, Singapore, 1997, p.157.
19. M.S. Hussein, A.F.R. de Toledo Piza, O.K. Vorov, and A.K. Kerman, Phys. Rev. **C60**, (1999), 064615.
20. B.A. Brown and P.G. Hansen, Phys. Lett. **381B** (1996) 391.
21. S. Karataglidis and C. Bennhold, Phys. Rev. Lett. **80** (1998) 1614.

22. Z.Z. Ren, A. Faessler, and A. Bobyk, Phys. Rev. **C57** (1998) 2752.
23. H. Sagawa and K. Yazaki, Phys. Lett. **B244** (1990) 149.
24. Ya.B. Zel'dovich, Zh.Exp.Teor.Fiz. **33** (1957) 1531 [Sov. Phys. JETP **6** (1957) 1184].
25. V.V. Flambaum and I.B. Khriplovich, Zh. Eksp. Teor. Fiz. **79** (1980) 1656 [Sov.Phys. JETP **52** (1980) 835]; V.V. Flambaum and I.B. Khriplovich and O.P. Sushkov, Phys. Lett. **B146** (1984) 367.
26. V.F. Flambaum and O.K. Vorov, Phys. Rev. Lett. **70** (1993) 4051.
27. V.F. Flambaum and O.K. Vorov, Phys. Rev. **C51** (1995) 1521.
28. N. Auerbach and B.A. Brown, Phys. Lett. **B340** (1994) 6.
29. W.C. Haxton, E.M. Henley, and M.J. Musolf, Phys. Rev. Lett. **63**, 949(1989).
30. C. Bouchiat and C.A. Piketty, Z. Phys. **C49** (1991) 91.
31. W.C. Haxton, Science, **275** (1997) 1753.
32. C.S. Wood, S.C. Bennet, D. Cho, B.P. Masterson, J.L. Roberts, C.E. Tanner, and C.E. Wieman, Science **275** (1997) 1759.
33. A. Bohr and B. Mottelson, *Nuclear Structure* (Benjamin, New York, 1969), Vol. 1.
34. T.T.S. Kuo, F. Krmpotic, and Y. Tzeng, Phys. Rev. Lett. **78** (1997) 2708.
35. V.V. Flambaum, I.B. Khriplovich, and O.P. Sushkov, Phys.Lett. **146B**, (1984), 367, Preprint INP-84-89; Phys. Lett. **B162**, (1985), 213; Nucl. Phys. **A449**, (1986), 750.
36. V.F. Dmitriev, I.B.Khriplovich and V.B. Telitsin, Nucl. Phys. **A577**, (1994), 691.
37. M.S. Noecker, B.P. Masterson and C.E. Wieman, Phys. Rev. Lett. **61**, (1988), 310.
38. W. Nazarewicz, J. Dobaczewski, and T.R. Werner, Phys. Scr. **T56**, (1995), 9.
39. D.J. Millener, J.W. Olness, E.K. Warburton, and S.S. Hanna, Phys. Rev. **C28**, (1983), 497.
40. F.M. Nunes, I.J. Thompson, and R.C. Johnson, Nucl. Phys. **A596**, (1996), 171; N.K. Timofeyuk and R.C. Johnson, Phys. Rev. **C59**, (1999), 1545.
41. S. Fortier et. al., Phys. Lett. **B461**, (1999), 22.